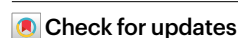


# NgR1 is an NK cell inhibitory receptor that destabilizes the immunological synapse

Received: 22 May 2022

Accepted: 22 November 2022

Published online: 09 January 2023



Se-Chan Oh<sup>1,2,10</sup>, Seong-Eun Kim<sup>3,10</sup>, In-Hwan Jang<sup>1,2</sup>, Seok-Min Kim<sup>1,2</sup>,  
Soo Yun Lee<sup>1</sup>, Sunyoung Lee<sup>1,4</sup>, In-Sun Chu<sup>5,6</sup>, Suk Ran Yoon<sup>1,2</sup>,  
Haiyoung Jung<sup>1,2</sup>, Inpyo Choi<sup>1</sup>, Junsang Doh<sup>7</sup>✉ & Tae-Don Kim<sup>1,2,8,9</sup>✉

The formation of an immunological synapse (IS) is essential for natural killer (NK) cells to eliminate target cells. Despite an advanced understanding of the characteristics of the IS and its formation processes, the mechanisms that regulate its stability via the cytoskeleton are unclear. Here, we show that Nogo receptor 1 (NgR1) has an important function in modulating NK cell-mediated killing by destabilization of IS formation. NgR1 deficiency or blockade resulted in improved tumor control of NK cells by enhancing NK-to-target cell contact stability and regulating F-actin dynamics during IS formation. Patients with tumors expressing abundant NgR1 ligand had poor prognosis despite high levels of NK cell infiltration. Thus, our study identifies NgR1 as an immune checkpoint in IS formation and indicates a potential approach to improve the cytolytic function of NK cells in cancer immunotherapy.

Cancer immunotherapy has been used for decades to eliminate tumors, and various types of immune cells have been used for the purpose, especially those that can lyse target cells via cell-to-cell contact<sup>1,2</sup>. NK cells are used in cancer immunotherapy owing to their natural properties; for instance, there are advantages of using allogeneic NK cells for adoptive transfer, and NK cells confer safety against cytokine release syndrome and can serve as first-line defenders for target cells<sup>3,4</sup>. NK cells form an IS, based on cell-to-cell contact, to recognize and eliminate virus-infected and transformed cancer cells<sup>5–8</sup>. The IS is a dynamic supramolecular structure, where spatiotemporal organization of cytoskeleton, surface receptors and intracellular signaling proteins occurs for signal integration and directed secretion of effector molecules<sup>7,9</sup>. NK cell IS formation is a multistep sequential event comprising initiation of a transient contact for target cell surveillance, establishment of firm adhesion mediated by adhesion molecules and

cytoskeleton remodeling, and polarization and excretion of lytic granules for target cell lysis<sup>10</sup>. Activating and inhibitory signals, integrated through the IS, determine target cell fates. Inhibitory signals typically work in the early stages of IS to interfere with activating signals that form and stabilize the IS through cytoskeleton remodeling, leading to NK–target interactions, thereby acting as immune checkpoints<sup>8,11</sup>. Existing immune checkpoint inhibitors do not ensure complete satisfactory outcomes in patients<sup>12,13</sup>; therefore, the discovery of novel inhibitory receptors would have notable scientific and clinical implications, as such receptors could be ideal targets for cancer immunotherapy.

The term IS originated from synapses of the nervous system, which have similar properties of cell-to-cell contact and signal transmission<sup>14</sup>. Guidance cues, including attractive and repulsive cues, are the key molecules regulating axonal outgrowth and synapse formation in the central nervous system (CNS)<sup>15,16</sup>. Among the many

<sup>1</sup>Immunotherapy Research Center, Korea Research Institute of Bioscience and Biotechnology, Daejeon, Republic of Korea. <sup>2</sup>Department of Functional Genomics, KRIBB School of Bioscience, Korea University of Science and Technology, Daejeon, Republic of Korea. <sup>3</sup>Department of Mechanical Engineering, Pohang University of Science and Technology, Pohang, Republic of Korea. <sup>4</sup>Department of Life Sciences, Korea University, Seoul, Republic of Korea. <sup>5</sup>Korea Research Institute of Bioscience and Biotechnology, Daejeon, Republic of Korea. <sup>6</sup>Department of Bioinformatics, KRIBB School of Bioscience, Korea University of Science and Technology, Daejeon, Republic of Korea. <sup>7</sup>Department of Materials Science and Engineering, Research Institute of Advanced Materials, Institute of Engineering Research, Bio-MAX Institute, Soft Foundry Institute, Seoul National University, Seoul, Republic of Korea. <sup>8</sup>Biomedical Mathematics Group, Institute for Basic Science, Daejeon, Republic of Korea. <sup>9</sup>Department of Biopharmaceutical Convergence, School of Pharmacy, Sungkyunkwan University, Suwon, Republic of Korea. <sup>10</sup>These authors contributed equally: Se-Chan Oh, Seong-Eun Kim.

✉e-mail: [jsdoh@snu.ac.kr](mailto:jsdoh@snu.ac.kr); [tdkim@kribb.re.kr](mailto:tdkim@kribb.re.kr)

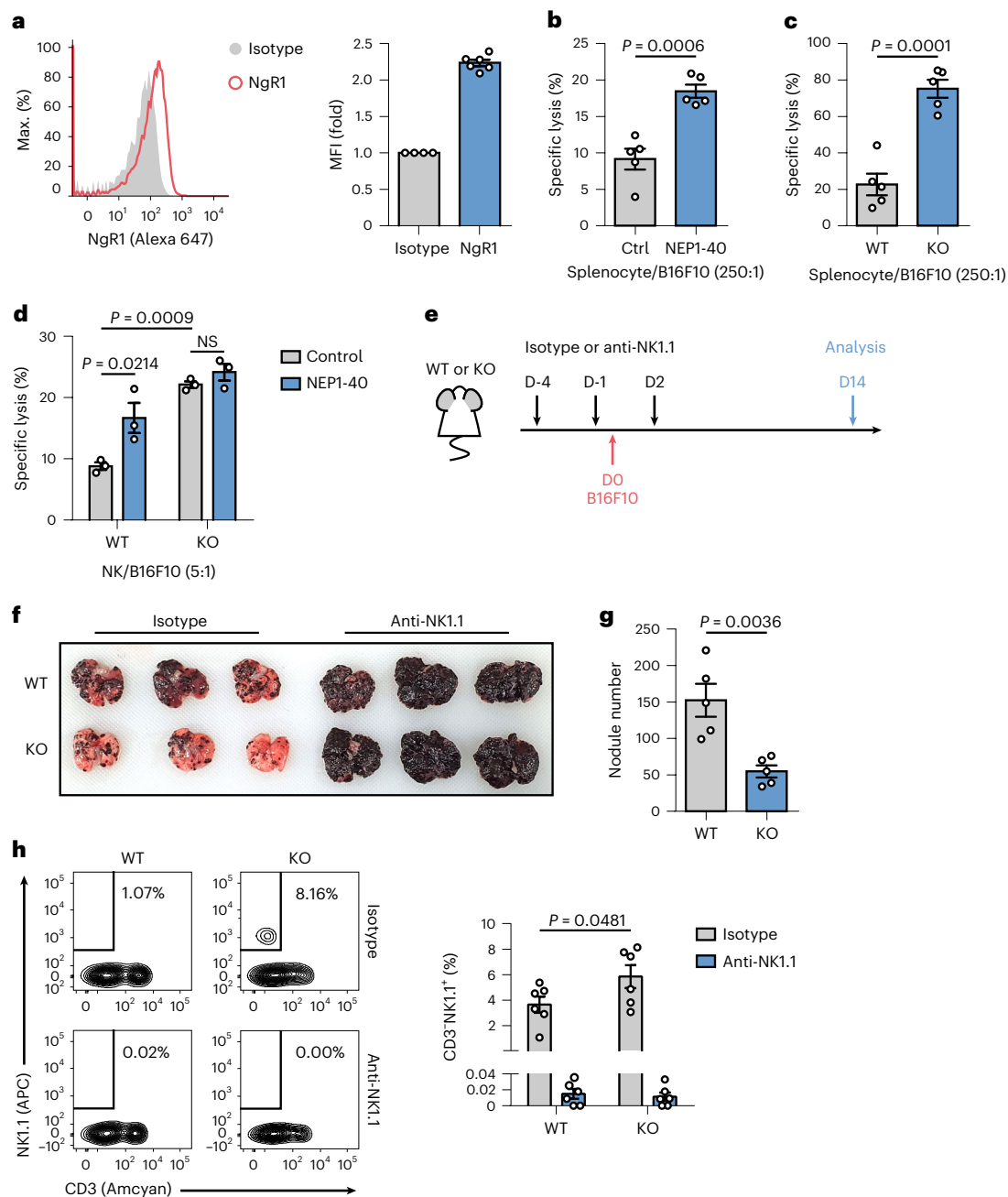


**Fig. 1 | NgR1 deficiency enhances NK cell killing in vitro and in vivo.**

**a**, Representative flow cytometric histograms and folds of MFI for NgR1 expression in splenic NK cells from WT mouse ( $n = 4$  isotype,  $n = 6$  NgR1). **b-d**, Analysis of cytotoxicity against B16F10 cells of splenocytes from WT mice with or without NEPI-40 treatment ( $n = 5$  each) (**b**), splenocytes from WT and KO mice ( $n = 5$  each) (**c**) and isolated splenic NK cells from WT and KO mice with or without NEPI-40 treatment ( $n = 3$  each) (**d**). **e**, Schematic of tumor and antibody administration for WT and KO mice. **f**, Representative lung images of WT and KO mice injected intravenously with isotype or NK1.1 antibody and B16F10

cells. **g**, Numbers of nodules formed in lungs of WT and KO mice ( $n = 5$  each). **h**, Representative flow cytometric plots and frequencies for intrapulmonary NK cells ( $CD3^+ NK1.1^+$ ) from WT and KO mice ( $n = 6$  each). In **a-d**, **g** and **h**, data represent mean  $\pm$  s.e.m. Data are representative of three independent experiments (**a**), two independent experiments (**b**, **c** and **d**) or one independent experiment from biologically independent samples (**g** and **h**). Statistical significance was calculated by unpaired two-tailed Student's *t* test (**b**, **c** and **g**) or two-way ANOVA with Tukey's multiple comparisons test (**d** and **h**). NS, not significant ( $P > 0.05$ ). Max., maximum. MFI, mean fluorescence intensity.

repulsive cues that function as inhibitors for axon growth and synaptic function, NgR1 has a well-established role in neurophysiopathology<sup>17,18</sup>. NgR1 consists of domains including leucine-rich repeat, stalk and glycosylphosphatidylinositol (GPI) and has high homology between humans and mice<sup>19</sup>. NgR1 recognizes its ligand, NogoA, and induces neuronal degeneration by RhoA signals that regulate actin cytoskeletal dynamics in damaged neurons<sup>20,21</sup>. NgR1 is also expressed in various immune cells and regulates their adhesion to myelin expressing NogoA, suggesting an immunomodulatory role

in neuroinflammation<sup>22</sup>. However, studies are limited to the nervous system, providing insufficient information about molecular mechanisms, and do not address the role of NgR1 in tumor control, which is a crucial function of immune cells. Therefore, defining the role of NgR1 in IS formation and the subsequent killing effects of NK cells is necessary to improve our understanding of the antitumor mechanism of NK cells.

Here, we report a modulatory function of NgR1 in the killing ability of NK cells against NogoA-expressing target cells via interference with

contact stability and complete IS formation. Moreover, the relationship between NogoA expression in tumors and NK cell infiltration indicates unfavorable clinical outcomes in patients. Taken together, these findings reveal an underlying mechanism of regulation of IS formation by NgR1, suggesting a potential target that could be used to improve cancer immunotherapy.

## Results

### NgR1 interferes with the antitumor function of NK cells

To assess the role of NgR1 in NK cells, we first investigated the cell surface expression of NgR1. We found NgR1 to be expressed in mouse primary NK cells, CD8 T cells and the EL4 cell line (Fig. 1a and Extended Data Fig. 1a). As the GPI-anchored receptor NgR1 lacks an endo-domain for intracellular signaling, it requires the participation of a complex of coreceptors, including immunoglobulin-like domain-containing protein 1 (LINGO1), tumor necrosis factor receptor superfamily member 19 (TROY) and neutrophin receptor (p75NTR)<sup>23,24</sup>. We found the coreceptors of NgR1 to be expressed in mouse primary splenic NK cells and the EL4 cell line (Extended Data Fig. 1b). As NK cells recognize the ligand and lyse cancer cells<sup>3,6</sup>, we confirmed the expression of NogoA, a ligand of NgR1, in various cancer cell lines (Extended Data Fig. 1c). Next, we measured the cell-mediated cytotoxicity of mouse splenocytes to investigate the involvement of NgR1 in the cytolytic function of immune cells. After treatment with NEPI-40, which is an antagonistic peptide of NgR1 (ref. 25), splenocytes of wild-type (WT) mice showed higher cytotoxicity than those of controls (Fig. 1b and Extended Data Fig. 1d). Moreover, we found that splenocytes from NgR1-knockout (KO) mice exhibited higher cytolytic effects than those from WT mice (Fig. 1c). To verify the specificity of NEPI-40 and determine whether the function of NgR1 is restricted to NK cells, we investigated the cytotoxicity of NK cells isolated from the spleens of WT and KO mice with or without NEPI-40 treatment. NK cells from KO mice showed higher cytotoxicity than those from WT mice, and only NK cells from WT mice showed increased cytotoxicity with NEPI-40 treatment (Fig. 1d). As NK cytotoxicity improved upon NgR1 deficiency, we hypothesized that WT and KO mice would exhibit different resistance to tumors. To verify this hypothesis, a syngeneic mouse model of lung metastasis was established for WT and KO mice (Fig. 1e). After intravenous administration of B16F10 cells, fewer metastatic nodules remained in the lungs of KO mice than in those of WT mice, but no difference was seen in the NK cell-depleted group, suggesting that the animal model was NK cell-dependent (Fig. 1f,g). As NK cell infiltration in tumors is an indicator of tumor resistance<sup>26,27</sup>, we investigated the population of intrapulmonary NK cells. The NK cell population (CD3<sup>+</sup>NK1.1<sup>+</sup>) that infiltrated the lungs bearing tumor nodules was greater in KO mice than in WT mice (Fig. 1h). These data suggest that NgR1 in NK cells contributes negatively to tumor control.

To investigate whether the improved antitumor effect caused by NgR1 deficiency was due to intrinsic alterations in immune composition, we analyzed the populations of immune cells from WT and KO mice. Total NK cells (CD3<sup>+</sup>NK1.1<sup>+</sup>) were classified into four maturation stages according to the expression of CD11b and CD27, namely immature NK cells (CD27<sup>−</sup>CD11b<sup>−</sup>), early mature NK cells (mNK; CD27<sup>+</sup>CD11b<sup>−</sup>), mNK cells (CD27<sup>+</sup>CD11b<sup>+</sup>) and late mNK cells (CD27<sup>−</sup>CD11b<sup>+</sup>)<sup>28</sup>. We found no difference between WT and KO mice in resting and IL-2-stimulated total or classified NK cell populations, or in IFN- $\gamma$  expression (Extended Data Fig. 2a–c). Populations of CD8 T cells (CD3<sup>+</sup>CD8<sup>+</sup>), CD4 T cells (CD3<sup>+</sup>CD4<sup>+</sup>), B cells (B220<sup>+</sup>), myeloid cells (CD11b<sup>+</sup>Gr1<sup>+</sup>), neutrophils (CD11b<sup>+</sup>Gr1<sup>high</sup>), monocytes (CD11b<sup>+</sup>Gr1<sup>low</sup>) and macrophages (CD11b<sup>+</sup>F4/80<sup>high</sup>) also showed no differences between WT and KO mice (Extended Data Fig. 2d–f). These data collectively indicate that NgR1 deficiency does not affect the composition of immune cells, implying that NgR1 is mainly involved in the effector function of NK cells.

### NgR1 regulates NK cell actin cytoskeleton dynamics

As NgR1 is involved in the tumor control of mouse NK cells, it might have a prominent role in human NK cells as well. To verify this, we investigated the expression of NgR1 and its signals in human NK cells. NgR1 was found to be expressed in human NK cells, including umbilical cord blood (UCB)-derived NK cells (UCB-NK), peripheral blood (PB)-derived NK cells (PB-NK), cytokine-induced mNK cells, NK92 cells, UCB-CD8 T cells and Jurkat cells (Fig. 2a and Extended Data Fig. 3a). We also found that the coreceptors of NgR1 were expressed in human UCB-NK, PB-NK, mNK, NK92 and Jurkat cell lines (Extended Data Fig. 3b). NgR1 is well known to recognize NogoA and activates cytoskeleton-regulatory signals<sup>20,29</sup>. With RhoA activation by NgR1 stimulation, Rho-associated coiled-coil-containing protein kinase (ROCK) phosphorylates LIM domain kinase 1 (LIMK1) and LIMK2 to phosphorylate and inactivate cofilin, which severs filamentous (F)-actin into globular (G)-actin<sup>18,20</sup>. To investigate the signaling of NgR1, we stimulated NgR1 in NK cells. Following treatment with Nogo-P4, an agonistic peptide of NgR1 (ref. 30), both RhoA and LIMK were activated and cofilin was inactivated in NK92 cells and UCB-NK cells (Fig. 2b and Extended Data Fig. 3c). RhoA activation promotes stress fiber formation through actomyosin-based contraction and cofilin inactivation, leading to actin cytoskeleton reorganization<sup>31,32</sup>. Accumulation of F-actin causes the formation of cell membrane protrusion, which affects cell migration and adhesion<sup>33</sup>. As NgR1 stimulation activates RhoA and inactivates cofilin, we hypothesized that NgR1 would affect the actin regulation of NK cells. To verify this, F-actin was directly visualized in NK92 cells expressing Lifeact-GFP, and the effects of Nogo-P4 treatment on F-actin dynamics were assessed by video microscopy. Nogo-P4-treated NK92 cells exhibited significantly increased F-actin intensity (Fig. 2c,d and Supplementary Video 1) and membrane protrusion frequency (Fig. 2c,e and Supplementary Video 1) compared with untreated (Ctrl) or scrambled peptide (Scram)-treated NK cells. Phalloidin staining of F-actin (Extended Data Fig. 4a,b,e,f) and membrane protrusion frequency measurements from bright field images (Extended Data Fig. 4c,d and Supplementary Video 2) using WT or Lifeact-GFP-expressing NK92 cells demonstrated identical results, indicating a minimal Lifeact-mediated artifact of F-actin dynamics<sup>34</sup> in NK92 cells. These data suggest that NgR1 in NK cells regulates actin cytoskeleton dynamics through RhoA signals.

### NgR1 regulates NogoA-mediated NK cell killing

To assess the NogoA-specificity of NgR1 in NK cell killing, we investigated NK cell-mediated cytotoxicity by regulating the function and expression of NgR1 in NK cells or NogoA in target cells. First, we confirmed the expression of NogoA in cancer cell lines. NogoA was expressed at different levels on the surfaces of the target cells (Extended Data Fig. 5a). Killing of NK92 cells relative to K562 cells, which hardly express NogoA, showed no difference with or without blocking of NgR1 with NEPI-40 (Fig. 3a). However, NK-mediated killing was significantly reduced for NogoA-overexpressing K562 cells and was rescued by NEPI-40 treatment, similar to the results in HEK293T cells (Fig. 3b,c and Extended Data Fig. 5b,c). After treatment with NEPI-40, there was increased NK cytotoxicity against U87MG cells, a glioma cell line from brain tumors known to express high levels of NogoA<sup>35</sup> (Fig. 3d). We further found that NK cytotoxicity increased upon inhibition of NogoA expression in U87MG cells or NgR1 expression in NK92 cells (Fig. 3e,f and Extended Data Fig. 5d–f). As NK cell activity depends on the balance between activating and inhibitory signals to kill the target<sup>3,5,11</sup>, we questioned whether NgR1 could be involved in killing NK cell-resistant targets. To verify this, we investigated the expression of activating and inhibitory ligands in several cell lines. AU565 cells expressed NogoA while expressing little or no activating ligand such as ULBP1, ULBP2, ULBP3 or MIC-A/B (Extended Data Fig. 5a,g). The cytotoxicity of NK cells against AU565 cells significantly increased owing to the blocking of NgR1 by NEPI-40 treatment (Fig. 3g). Similar to NK92 cells, human

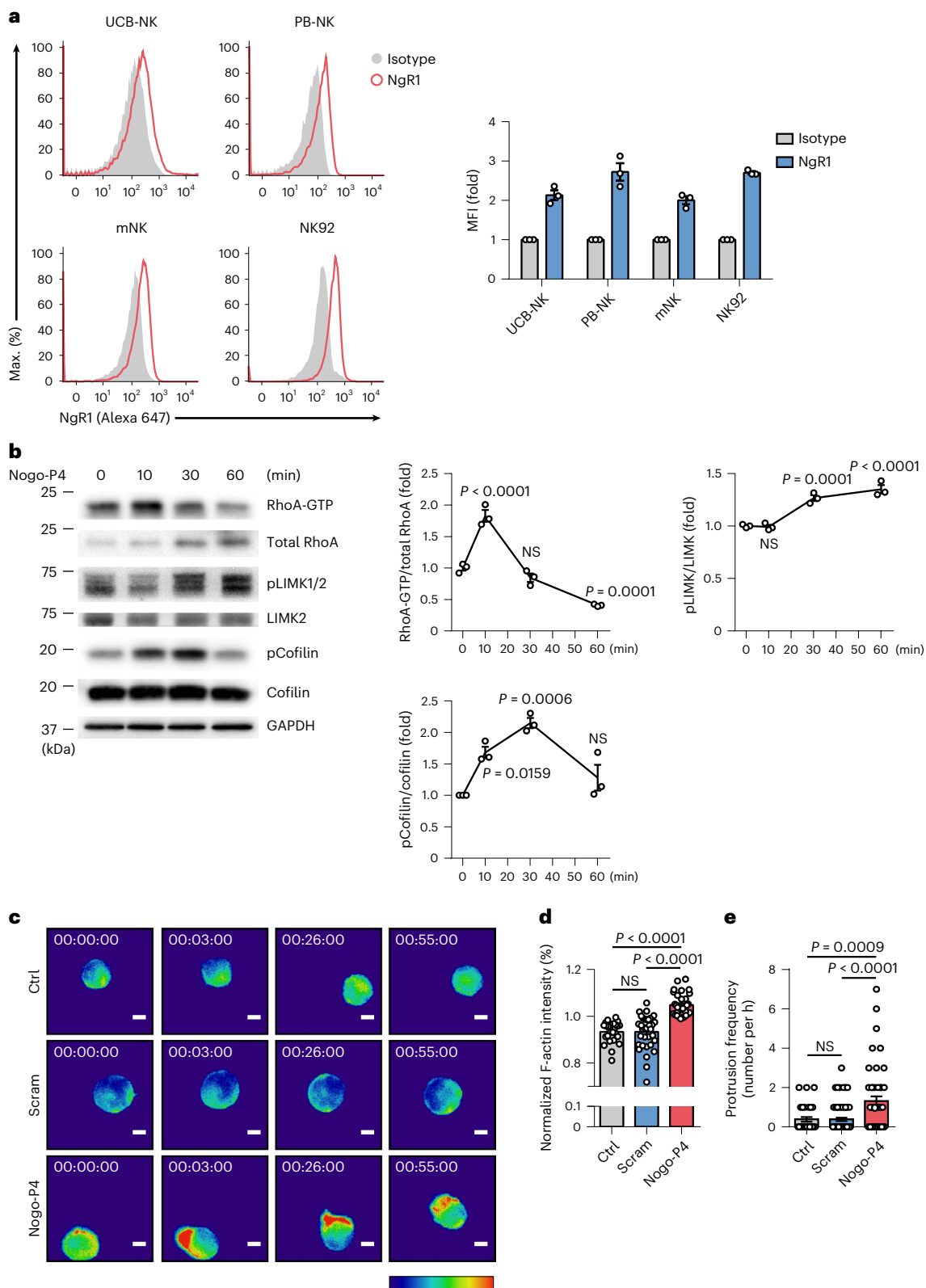


**Fig. 2 | NgR1 promotes F-actin polymerization in NK cells. a**, Representative flow cytometric histograms and folds of MFI for NgR1 expression in human UCB-NK, PB-NK, mNK and NK92 cells ( $n = 3$  each). **b**, Representative immunoblots and quantification analysis of lysate from NK92 cells treated with Nogo-P4 for the indicated times ( $n = 3$  each). **c**, Time-lapse images of fluorescence intensity of NK92 cells expressing Lifeact-GFP with Ctrl, Scram or Nogo-P4 treatment using video fluorescence microscopy. Fluorescence intensity was visualized with a

pseudocolor rainbow scale. Scale bar, 5  $\mu$ m. **d,e**, Single-cell analysis of relative F-actin intensity ( $n = 26$  Ctrl;  $n = 34$  Scram;  $n = 33$  Nogo-P4) (**d**) and protrusion frequency ( $n = 31$  Ctrl;  $n = 65$  Scram;  $n = 50$  Nogo-P4) (**e**). In **a**, **b**, **d** and **e**, data represent mean  $\pm$  s.e.m. (**a**, **d** and **e**) or mean  $\pm$  s.d. (**b**). Data are representative of three independent experiments (**a**) or two independent experiments (**b**, **d** and **e**). Statistical significance was calculated by one-way ANOVA with Tukey's multiple comparisons test (**b**, **d** and **e**).

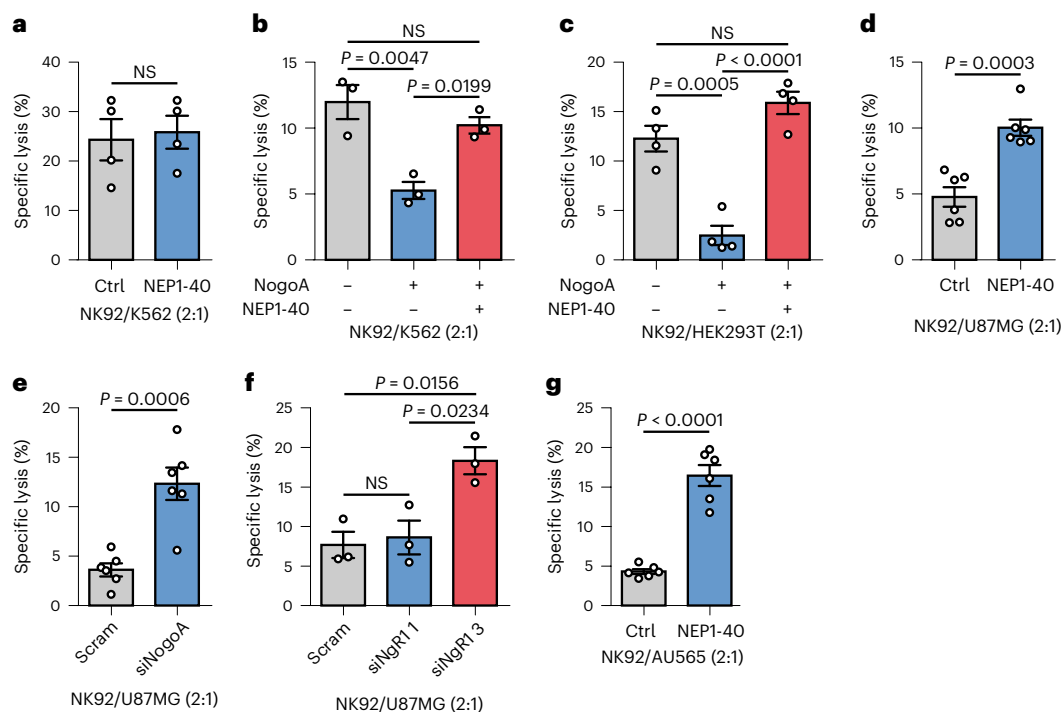


**Fig. 3 | NK cell-mediated cytotoxicity is suppressed in a NogoA–NgR1-dependent manner.** **a–d**, Cytotoxicity analysis of NK92 cells against K562 cells ( $n = 4$  each) (**a**), NogoA-overexpressing K562 cells ( $n = 3$  each) (**b**), NogoA-overexpressing HEK293T cells ( $n = 4$  each) (**c**) and U87MG cells ( $n = 6$  each) (**d**) with and without NEPI-40 treatment. **e**, Cytotoxicity analysis of NK92 cells against U87MG cells with suppressed NogoA expression ( $n = 6$  each). **f**, Cytotoxicity analysis of NK92 cells with suppressed expression of NgR1 against

U87MG cells ( $n = 3$  each). **g**, Cytotoxicity analysis of NK92 cells against AU565 cells with and without NEPI-40 treatment ( $n = 6$  each). In **a–g**, data represent mean  $\pm$  s.e.m. Data are representative of six independent experiments (**d**, **e** and **g**) four independent experiments (**c**) or three independent experiments (**a**, **b** and **f**). Statistical significance was calculated by unpaired two-tailed Student's *t* test (**a**, **d**, **e** and **g**) or one-way ANOVA with Tukey's multiple comparisons test (**b**, **c** and **f**).

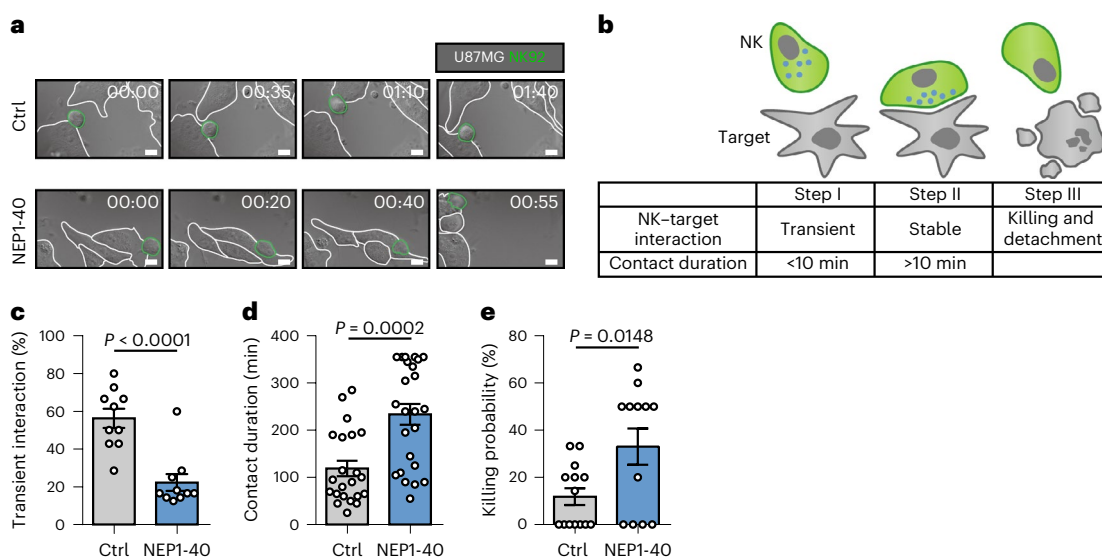


**Fig. 4 | NgR1 blockade positively regulates NK-to-target contact at an early stage.** **a**, Representative time-lapse images of interactions between NK92 (green border line) and U87MG cells (white border line) with and without NEPI-40 treatment. Scale bar, 10  $\mu$ m. **b**, Schematic of steps for NK–target interaction. **c–e**, Effects of NEPI-40 on NK92 transient interaction frequencies ( $n = 10$  each)

(**c**), contact duration time ( $n = 22$  Ctrl,  $n = 24$  NEPI-40) (**d**) and killing probability ( $n = 14$  Ctrl,  $n = 12$  NEPI-40) (**e**). In **c–e**, the data represent mean  $\pm$  s.e.m. Data are representative of three independent experiments (**c–e**). Statistical significance was calculated by unpaired two-tailed Student's *t* test (**c–e**).

UCB-NK and PB-NK cells showed increased killing upon blocking of NgR1 (Extended Data Fig. 5h–i). Therefore, the data collectively suggest that NgR1 acts as an inhibitor of the cytolytic function of NK cells, specifically in the presence of NogoA.

#### NK-to-target cell contact is destabilized by NgR1

To further gain insight into how NgR1 signaling inhibits NK cell cytotoxicity, we directly observed interactions between NK and target cells by live-cell imaging. Most of the control NK92 cells transiently

interacted with U87MG cells (top panel of Fig. 4a and Supplementary Video 3), whereas a large fraction of NEPI-40-treated NK92 cells made stable contact with U87MG cells, and some NK92 cells eventually killed U87MG cells (bottom panel of Fig. 4a and Supplementary Video 3). Typically, NK cells transiently interact with target cells to scan their surfaces (step I in Fig. 4b) and then form stable synapses (step II in Fig. 4b) that direct the polarized secretion of lytic granules to perform target cell lysis (step III in Fig. 4b). We analyzed the percentage of NK92 cells transiently interacting with target cells with a contact duration <10 min and measured the contact duration between NK92 cells and target cells forming stable synapses. NEPI-40-treatment was found to significantly reduce transient interactions and increase contact duration, resulting in enhanced cytotoxicity (Fig. 4c–e). Similar results were obtained with human PB-NK or mouse NK cells when NgR1 was either blocked by NEPI-40 (Extended Data Fig. 6a–h and Supplementary Videos 4 and 5) or genetically knocked out (Extended Data Fig. 6i–l and Supplementary Video 6). Together, these results indicate that NgR1 signaling reduces NK cell cytotoxicity by interfering with stable synapse formation.

### F-actin dynamics are regulated by NgR1 during IS formation

NgR1 signaling is responsible for altering the actin cytoskeletal balance<sup>20,29</sup>. To investigate the molecular mechanism of NgR1 signals regulating NK-to-target contact, we regulated ROCK or LIMK activity or cofilin expression (Fig. 5a). As cofilin directly regulates F-actin dynamics<sup>20,31,32</sup>, we hypothesized that inhibition of cofilin expression would affect F-actin turnover, resulting in impairment of NK cell contact and subsequent killing. To verify this, we suppressed the expression of cofilin in NK92 cells with small interfering RNA (siRNA) (Extended Data Fig. 7a) and found that NK92–U87MG conjugation was reduced and NK killing was impaired (Fig. 5b,c). Next, we investigated NK-to-target contact and NK killing by treating NK cells with LIMKi3 (a LIMK1 and LIMK2 inhibitor). Nogo-P4-treated NK92 cells increased phosphorylation of LIMK and cofilin, whereas LIMKi3 treatment inhibited both LIMK phosphorylation and subsequent cofilin phosphorylation (Extended Data Fig. 7b). Moreover, we found that inhibition of LIMK and cofilin phosphorylation occurred through LIMK inhibition under NogoA-expressing U87MG cell-mediated NgR1 stimulation of NK92 cells (Fig. 5d). The contact between NK92 and U87MG cells following inhibition of LIMK was directly observed via live-cell imaging. Similar to NgR1 blockade or KO, LIMKi3 treatment significantly stabilized NK–target contacts, leading to enhanced cytotoxicity of NK cells (Fig. 5e–h and Supplementary Video 7). In addition, we confirmed the effect of the NgR1 signal on NK-mediated killing by regulating ROCK, an upstream signal of LIMK–cofilin. The cytotoxicity of NK92 cells against U87MG cells increased under NEPI-40 or H-1152 (ROCK inhibitor) treatment (Fig. 5i). As NK cell activation induces F-actin reorganization and IS formation via actin-regulating factors such as WASp and Arp2/3 (refs. 36,37), we compared these factors with the NgR1 signal. The cytotoxicity of NK92 cells against K562 was not changed even under treatment with NEPI-40. However, the cytotoxicity of NK92 cells was decreased by treatment with wiskostatin (a WASp inhibitor) or CK-666 (an Arp2/3 inhibitor), and there was no change upon cotreatment with NEPI-40 (Fig. 5j,k). The cytotoxicity of NK92 cells against U87MG increased under NEPI-40 treatment. Although the cytotoxicity of NK92

cells was decreased by treatment with wiskostatin or CK-666, it was restored by cotreatment with NEPI-40 (Fig. 5l,m). These data suggest that both activation and NgR1 signals of NK cells, which regulate IS formation with actin dynamics, influence NK cytotoxicity.

Next, we visualized F-actin dynamics in the context of IS using NK92 cells expressing Lifeact-GFP. F-actin polymerization at the IS is among the early events that are critical for stable IS formation<sup>7,8</sup>. In the control group, NK92 cells contacting U87MG cells mainly polarized F-actin outward from NK-to-target contacts and frequently detached from the target cells (top panel of Fig. 6a and Supplementary Video 8). By contrast, NEPI-40-treated NK92 cells polarized F-actin toward the NK-to-target contacts and maintained stable IS formation (bottom panel of Fig. 6a and Supplementary Video 8). F-actin distributions with respect to NK-to-target contacts were classified into four cases and were plotted for NK92–U87MG conjugates after the initiation of coculture (Fig. 6b). In the control group, the majority of NK92 cells polarized F-actin outward from the NK-to-target contacts, whereas in the NEPI-40-treated group, most NK92 cells polarized F-actin toward the NK–target contacts (Fig. 6b). NgR1 signaling also influenced lytic granule convergence and polarization toward the NK–target contacts, both of which are critical events for cytotoxicity (Fig. 6c,d and Supplementary Video 9); the majority of NK92 cells in the control group exhibited diffuse patterns of granules, indicating their failure to converge the granules. By contrast, most NK92 cells treated with NEPI-40 converged the lytic granules to the distal pole (approximately 50% in 30 min) and then polarized them toward the IS (approximately 80% in 120 min). Together, these results indicate that suppressed F-actin dynamics, mediated by NgR1 signaling at NK-to-target contacts, promote F-actin polymerization outward from the cell-to-cell contacts, resulting in the detachment of NK92 cells before lytic granule polarization toward IS.

### NgR1 functions as an immune checkpoint in NK cells

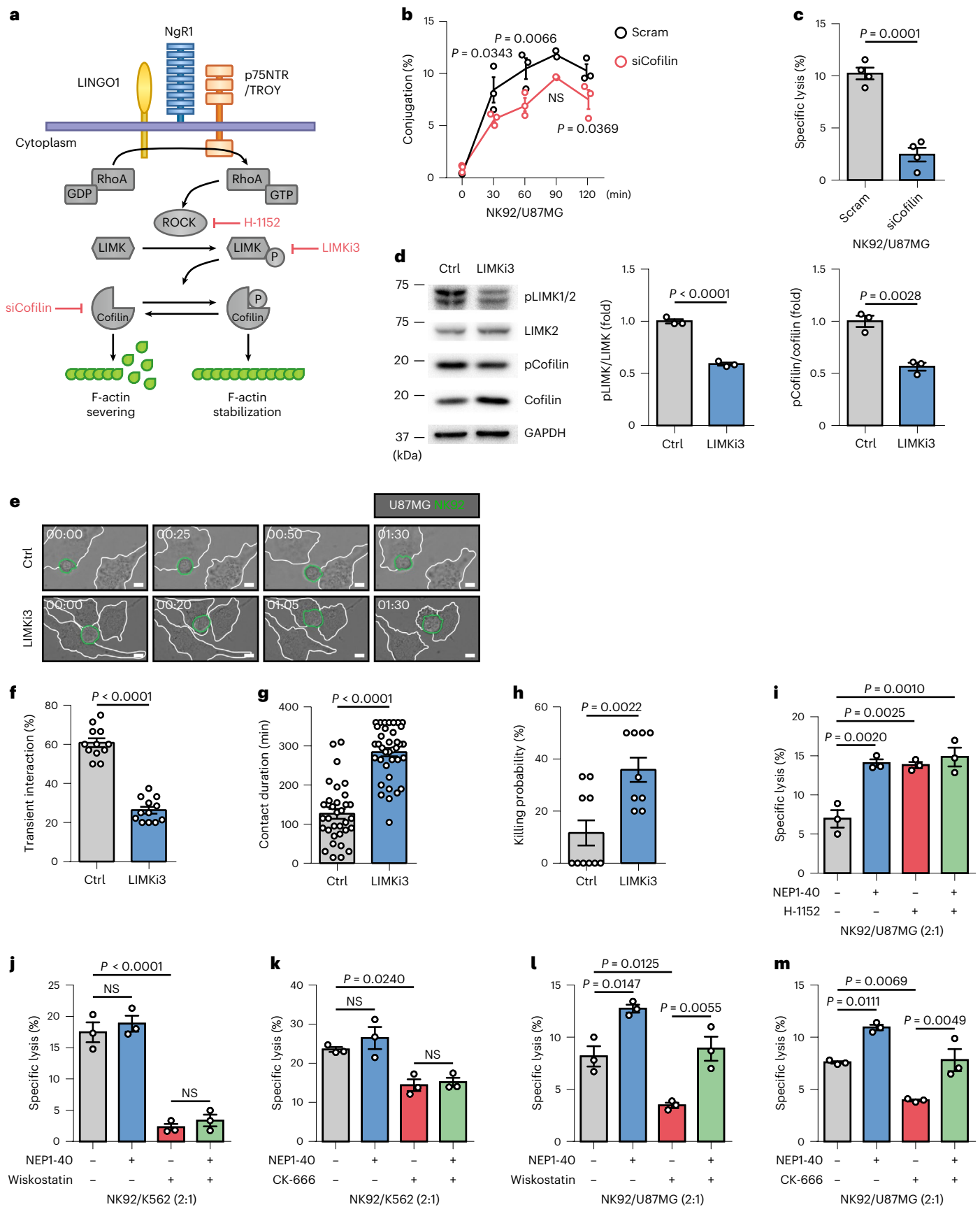
Considering that NK cells perform immune surveillance and NgR1 inhibits the cytolytic function of NK cells, the therapeutic effect of NgR1 blockade was investigated using a xenograft mouse model. Following subcutaneous injection of U87MG cells, NSIG mice were intravenously injected with NK92 cells on days 10 and 14, and scrambled peptide or NEPI-40 was injected intratumorally on days 11 and 15 (Fig. 7a). Tumor size was decreased in the group where NK92 cells and NEPI-40 were administered, compared with the group injected with phosphate-buffered saline (PBS; control) and NK92 cells with scrambled peptide (NK92) (Fig. 7b,c). Survival rates of tumor-bearing mice were improved in the group receiving NK92 cells with NEPI-40 (Fig. 7d). We next assessed whether NgR1 could be linked to clinical outcomes along with a relationship with *RTN4*, the gene encoding Nogo, in patients with cancer. First, rich- or poor-NK-infiltration groups were divided using CIBERSORT, and then clinical prognosis was deduced by grouping of patients with high or low *RTN4* expression using The Cancer Genome Atlas (TCGA) pan-cancer data (Fig. 7e). In all cancer patients, regardless of the quantity of infiltrated NK cells, we confirmed that *RTN4* was a risk factor for mortality and that high *RTN4* led to poor clinical outcomes (Fig. 7f,g, Extended Data Fig. 8a and Supplementary Table 1). In particular, the *RTN4* expression level of NK-rich patients represented a higher risk for overall survival

**Fig. 5 | NgR1 signals involve regulation of NK–target contact.** **a**, Schematic of downstream signals and inhibitors of NgR1. **b**, Conjugation frequencies between NK92 cells transfected with siCofilin and U87MG cells ( $n = 3$  each). **c**, Analysis of cytotoxicity on U87MG cells of NK92 cells transfected with siCofilin ( $n = 4$  each). **d**, Representative immunoblots and quantification analysis of lysate from NK92 cells with and without LIMKi3 treatment incubated with U87MG cells ( $n = 3$  each). **e**, Representative time-lapse images of interactions between NK92 cells (green border line) with and without LIMKi3 treatment and U87MG cells (white border line). Scale bar, 10  $\mu\text{m}$ . **f–h**, Effects of LIMKi3 on NK transient interaction frequencies ( $n = 12$  each) (**f**), contact duration time ( $n = 34$  Ctrl,  $n = 37$  LIMKi3) (**g**)

and killing probability ( $n = 10$  Ctrl,  $n = 9$  LIMKi3) (**h**). **i**, Analysis of cytotoxicity of NK92 cells to U87MG cells with and without NEPI-40 or H-1152 ( $n = 3$  each). **j–m**, Analysis of cytotoxicity of NK92 cells to K562 cells ( $n = 3$  each) (**j,k**) or U87MG cells ( $n = 3$  each) (**l,m**) with and without NEPI-40, wiskostatin or CK-666. In **b–d** and **f–m**, data represent mean  $\pm$  s.e.m. (**b,c** and **f–m**) or mean  $\pm$  s.d. (**d**). Data are representative of three independent experiment (**i–m**) or two independent experiments (**b–d** and **f–h**). Statistical significance was calculated by two-way ANOVA with Sidak's multiple comparisons test (**b**), unpaired two-tailed Student's *t* test (**c,d** and **f–h**) or one-way ANOVA with Tukey's multiple comparisons test (**i–m**).

than NK-poor patients. CD8 T cells showed similar results with respect to clinical outcomes and risk analysis for survival (Extended Data Fig. 8b–d and Supplementary Table 2). Collectively, these data

suggest that NgR1 expression in cytolytic immune cells serves as an immune checkpoint to inhibit IS formation and could represent a novel therapeutic target for controlling tumors (Fig. 7h).



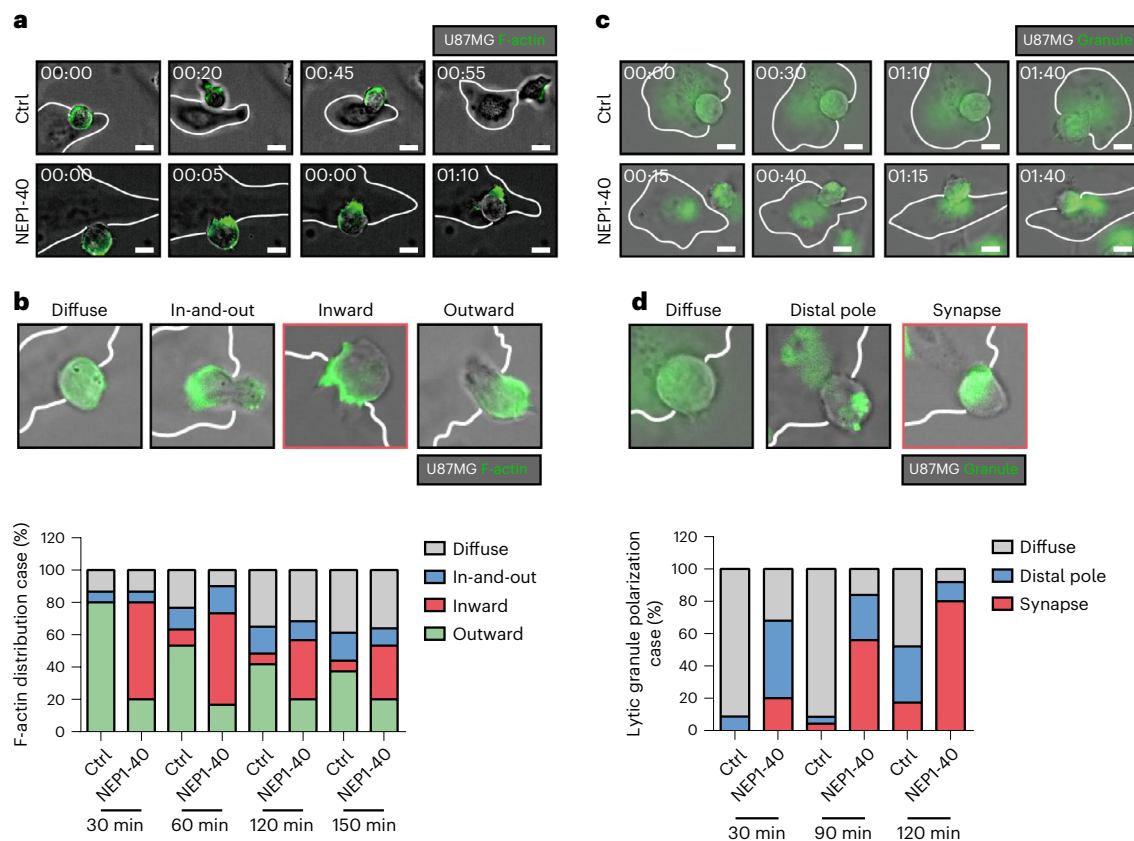


**Fig. 6 | An IS is stably formed by NgR1 blockade.** **a**, Representative time-lapse images obtained during incubation of Lifeact-GFP-expressing NK92 cells (green) and U87MG cells (white border line) with Ctrl and NEPI-40 treatment. Scale bar, 10  $\mu$ m. **b**, Representative images of F-actin distribution cases (upper panel) and frequency analysis (bottom panel) in NK92 cells (green) cultured with U87MG cells (white border line) for the indicated times with and without

NEPI-40 treatment. **c**, Representative time-lapse images of lytic granules in NK92 cells (green) incubated with U87MG cells (white border line) under Ctrl and NEPI-40 treatments. Scale bar, 10  $\mu$ m. **d**, Representative images of lytic granule polarization cases (upper panel) and frequency analysis (bottom panel) in NK92 cells (green) cultured with U87MG cells (white border line) for the indicated times with and without NEPI-40 treatment.

## Discussion

In this study, we identified NgR1 as a novel NK cell inhibitory receptor prohibiting stable IS formation by LIMK-cofilin-mediated alteration of actin dynamics. NgR1 deficiency or blockade promoted the stable formation of IS, thereby increasing NK cell killing and tumor control. Even when NK cells were infiltrated, patients with cancer expressing abundant Nogo still had poor prognosis. This revealed the underlying mechanism of improvement of NK cell function by NgR1 and highlighted the clinical finding that NgR1 acts as an immune checkpoint.

In the CNS, axonal growth and synapse formation are critical for signal transmission of neurons. In contrast to attractive cues promoting axon outgrowth and synapse formation by Rac1, and CDC42 signals promoting cytoskeleton dynamics, inhibitory cues interfere with axonal growth and synaptic function via RhoA signals that suppress cytoskeleton remodeling<sup>15,16</sup>. Neuronal growth inhibitors interfere with synapse formation by inducing axon growth cone collapse and retraction<sup>15,16,18</sup>. Among the inhibitory cues, NogoA–NgR1 interaction, which belongs to the myelin-associated inhibitor category, inhibits axonal growth and synaptic function through RhoA-mediated cytoskeleton regulation and is required to prevent abnormal neuronal sprouting in healthy brain and for neuronal degeneration upon CNS damage<sup>18,21,29</sup>. NgR1 acts as an inhibitory receptor that directly regulates neurons rather than blocking signals of attractive cues<sup>38,39</sup>. Recently, NgR1 has been reported to inhibit the adhesion of immune cells<sup>40</sup>; however, this is restricted to the nervous system and detailed mechanisms are missing. Elucidating the role of NgR1, which is otherwise well defined in the nervous system, in tumor control by immune cells is necessary to

obtain a better understanding of the mechanism of action of immune cells. This, in turn, could contribute to improving the performance of cancer immunotherapy.

NK cells form IS with target cells to identify infected and/or transformed cells and exert cytotoxicity. Synapse-mediated cytotoxicity is accomplished via stepwise processes, including tethering, F-actin accumulation, firm adhesion, granule convergence to microtubule organizing center (MTOC), MTOC polarization to IS and granule exocytosis<sup>8</sup>. Signaling mediated by inhibitory receptors, such as NKG2A and KIR, acts primarily in the early stages of IS to prevent activating signals from occurring<sup>8,11</sup>. Functionally, inhibitory receptor signals destabilize the IS and promote NK cell detachment and migration<sup>41</sup>. The characteristics of NgR1-mediated NK cell inhibition observed in this study were similar to those of inhibitory receptors; in the presence of NgR1–NogoA interactions, NK cells exhibited transient interactions with target cells and failed to polarize F-actin and lytic granules toward the IS, resulting in impaired cytotoxicity. However, NgR1 is distinct from other inhibitory receptors owing to the downstream signals that it triggers. Typically, inhibitory receptors recognize either major histocompatibility complex class I (MHC I) or non-MHC I ligands and signal through immunoreceptor tyrosine-based inhibitory motifs (ITIMs) located at their cytoplasmic tails, thereby blocking the activating signals<sup>11,13</sup>. NgR1, on the other hand, interacts with NogoA and signals through coreceptors, as it is a GPI-anchored receptor with no cytoplasmic domain<sup>29</sup>. In addition, NgR1 inhibits actin reorganization through RhoA GTPase, in contrast to activation signals such as NKG2D, which activate GTPases including CDC24, Rac1, and Vav1 that are favorable

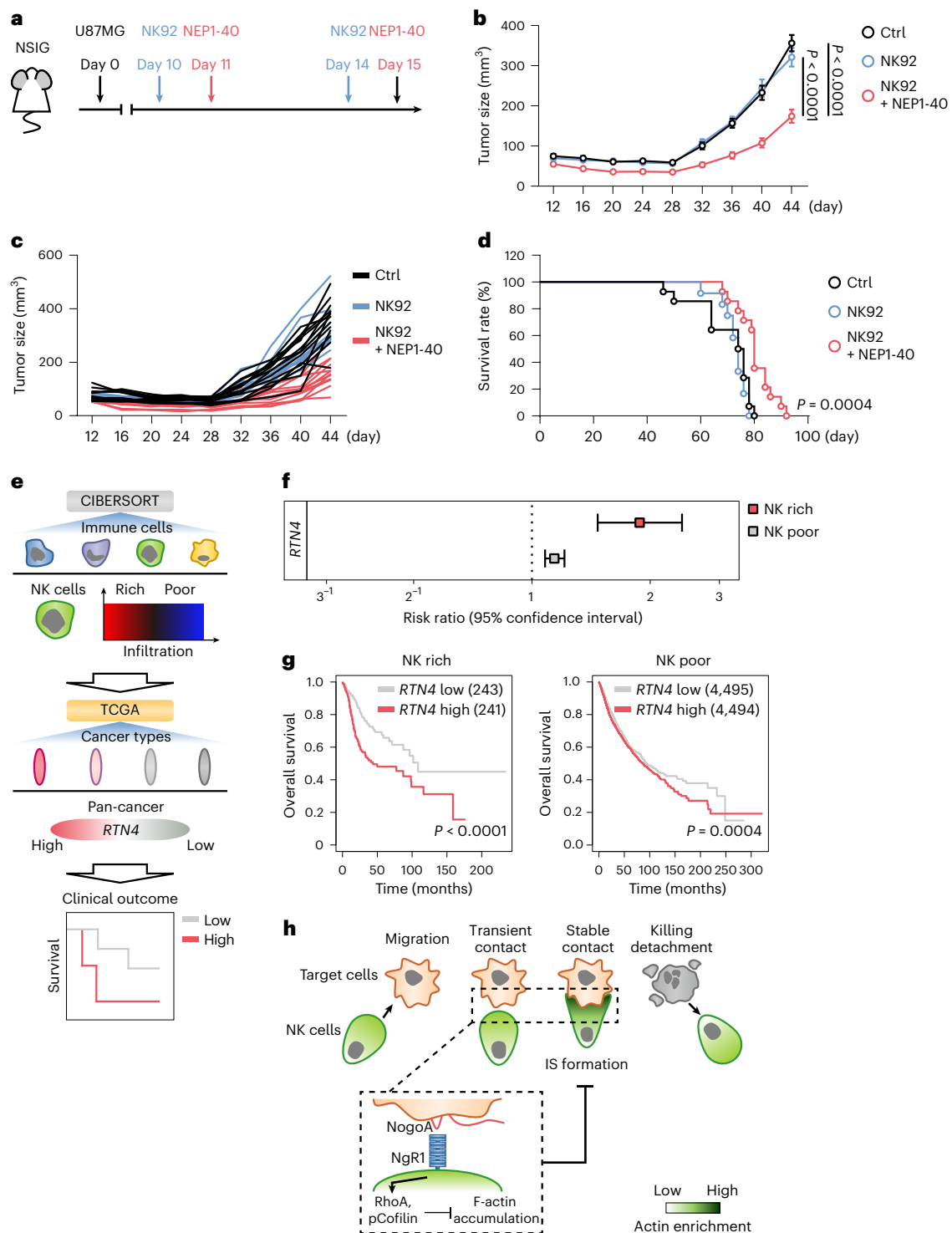


**Fig. 7 | NgR1 is a negative regulator in tumor control.** **a**, Schematic of administration of tumors, NK92 and peptide to NS1G mice. **b,c**, Average (**b**) and individual (**c**) tumor sizes in each condition ( $n = 14$  Ctrl,  $n = 11$  NK92,  $n = 14$  NK92 + NEP1-40). **d**, Survival rates in indicated conditions ( $n = 11$  Ctrl,  $n = 12$  NK92,  $n = 14$  NK92 + NEP1-40). **e**, Diagram of immune-cell-dependent survival analysis in large-scale cancer types profiled from TCGA. **f**, Cox hazard ratios of *RTN4* expression levels stratified by quantity of top 20% of NK cells infiltrated in TCGA

pan-cancer. **g**, Kaplan-Meier plot of *RTN4* expression level for top 20% NK-rich and bottom 80% NK-poor groups. **h**, Schematic cartoon showing the role of NgR1 in NK cells. In **b** and **f**, data represent mean  $\pm$  s.e.m. Data are representative of three independent experiments (**b** and **d**). Statistical significance was calculated by two-way ANOVA with Sidak's multiple comparisons test (**b**), log-rank test (**d** and **g**) or Wald test (**f**).

for IS formation<sup>18,37,42</sup>. Recently, immune checkpoint inhibitors have been developed to improve the tumor-killing ability of immune cells; however, challenges such as application to specific cancer types, recurrence or resistance still exist<sup>12,13</sup>. It is not yet clear whether blocking the

activating signals through ITIMs is the only mechanism that regulates actin dynamics and prevents IS formation in NK cells<sup>10</sup>. Therefore, the discovery of NgR1 as an inhibitory receptor broadens the range of NK inhibitory receptors.

Although the role of actin cytoskeleton remodeling mediated by the RhoA–ROCK–LIMK–cofilin axis, downstream of NgR1 signaling, has been well established in neural synapse<sup>18,21,29</sup>, it has not been investigated in IS. Although RhoA-mediated inhibition of T cell and NK cell cytotoxicity<sup>43,44</sup> and cofilin-mediated T cell synapse formation for T cell activation<sup>44,45</sup> have previously been reported, upstream signals activating RhoA and deactivating cofilin have not yet been identified. For ITIM-mediated actin remodeling in NK cells that leads to synaptic destabilization, dephosphorylation of Vav1 (ref. 46), a guanine nucleotide exchange factor important for immune cell activation, and phosphorylation of the adapter protein Crk<sup>47</sup> have primarily been considered<sup>10</sup>. It would be interesting to see whether the pathway identified in this study is also triggered in ITIM-mediated NK cell suppression. In addition, as RhoA and Rac1 interfere with each other, the detailed relationship of these signals<sup>48</sup>, which are spatiotemporally involved in NK killing, should also be elucidated. Overall, our preliminary results reveal that CD8<sup>+</sup> T cells express NgR1, and that NgR1-mediated signaling inhibits T cell-mediated cytotoxicity, implying that NgR1 could be a crucial inhibitory checkpoint for our immune system.

## Online content

Any methods, additional references, Nature Portfolio reporting summaries, source data, extended data, supplementary information, acknowledgements, peer review information; details of author contributions and competing interests; and statements of data and code availability are available at <https://doi.org/10.1038/s41590-022-01394-w>.

## References

- Smyth, M. J., Godfrey, D. I. & Trapani, J. A. A fresh look at tumor immunosurveillance and immunotherapy. *Nat. Immunol.* **2**, 293–299 (2001).
- Hiam-Galvez, K. J., Allen, B. M. & Spitzer, M. H. Systemic immunity in cancer. *Nat. Rev. Cancer* **21**, 345–359 (2021).
- Guillerey, C., Huntington, N. D. & Smyth, M. J. Targeting natural killer cells in cancer immunotherapy. *Nat. Immunol.* **17**, 1025–1036 (2016).
- Liu, S. et al. NK cell-based cancer immunotherapy: from basic biology to clinical development. *J. Hematol. Oncol.* **14**, 7 (2021).
- Cerwenka, A. & Lanier, L. L. Natural killer cells, viruses and cancer. *Nat. Rev. Immunol.* **1**, 41–49 (2001).
- Vivier, E., Tomasello, E., Baratin, M., Walzer, T. & Ugolini, S. Functions of natural killer cells. *Nat. Immunol.* **9**, 503–510 (2008).
- Davis, D. M. Assembly of the immunological synapse for T cells and NK cells. *Trends Immunol.* **23**, 356–363 (2002).
- Mace, E. M. et al. Cell biological steps and checkpoints in accessing NK cell cytotoxicity. *Immunol. Cell Biol.* **92**, 245–255 (2014).
- Dustin, M. L. & Baldari, C. T. The immune synapse: past, present, and future. *Methods Mol. Biol.* **1584**, 1–5 (2017).
- Ben-Shmuel, A., Sabag, B., Biber, G. & Barda-Saad, M. The role of the cytoskeleton in regulating the natural killer cell immune response in health and disease: from signaling dynamics to function. *Front. Cell Dev. Biol.* **9**, 609532 (2021).
- Long, E. O., Kim, H. S., Liu, D., Peterson, M. E. & Rajagopalan, S. Controlling natural killer cell responses: integration of signals for activation and inhibition. *Annu. Rev. Immunol.* **31**, 227–258 (2013).
- Topalian, S. L., Drake, C. G. & Pardoll, D. M. Immune checkpoint blockade: a common denominator approach to cancer therapy. *Cancer Cell* **27**, 450–461 (2015).
- Qin, S. et al. Novel immune checkpoint targets: moving beyond PD-1 and CTLA-4. *Mol. Cancer* **18**, 155 (2019).
- Norcross, M. A. A synaptic basis for T-lymphocyte activation. *Ann. Immunol.* **135D**, 113–134 (1984).
- Sharma, K., Selzer, M. E. & Li, S. Scar-mediated inhibition and CSPG receptors in the CNS. *Exp. Neurol.* **237**, 370–378 (2012).
- Omotade, O. F., Pollitt, S. L. & Zheng, J. Q. Actin-based growth cone motility and guidance. *Mol. Cell Neurosci.* **84**, 4–10 (2017).
- Strittmatter, S. M. Modulation of axonal regeneration in neurodegenerative disease: focus on Nogo. *J. Mol. Neurosci.* **19**, 117–121 (2002).
- Pernet, V. & Schwab, M. E. The role of Nogo-A in axonal plasticity, regrowth and repair. *Cell Tissue Res.* **349**, 97–104 (2012).
- Saha, N., Kolev, M. & Nikolov, D. B. Structural features of the Nogo receptor signaling complexes at the neuron/myelin interface. *Neurosci. Res.* **87**, 1–7 (2014).
- Niederost, B., Oertle, T., Fritsche, J., McKinney, R. A. & Bandtlow, C. E. Nogo-A and myelin-associated glycoprotein mediate neurite growth inhibition by antagonistic regulation of RhoA and Rac1. *J. Neurosci.* **22**, 10368–10376 (2002).
- Schwab, M. E. & Strittmatter, S. M. Nogo limits neural plasticity and recovery from injury. *Curr. Opin. Neurobiol.* **27**, 53–60 (2014).
- Seiler, S., Di Santo, S. & Widmer, H. R. Non-canonical actions of Nogo-A and its receptors. *Biochem. Pharmacol.* **100**, 28–39 (2016).
- Mi, S. et al. LINGO-1 is a component of the Nogo-66 receptor/p75 signaling complex. *Nat. Neurosci.* **7**, 221–228 (2004).
- Park, J. B. et al. A TNF receptor family member, TROY, is a coreceptor with Nogo receptor in mediating the inhibitory activity of myelin inhibitors. *Neuron* **45**, 345–351 (2005).
- GrandPre, T., Li, S. & Strittmatter, S. M. Nogo-66 receptor antagonist peptide promotes axonal regeneration. *Nature* **417**, 547–551 (2002).
- Vesely, M. D., Kershaw, M. H., Schreiber, R. D. & Smyth, M. J. Natural innate and adaptive immunity to cancer. *Annu. Rev. Immunol.* **29**, 235–271 (2011).
- Cozar, B. et al. Tumor-Infiltrating natural killer cells. *Cancer Discov.* **11**, 34–44 (2021).
- Chiossone, L. et al. Maturation of mouse NK cells is a 4-stage developmental program. *Blood* **113**, 5488–5496 (2009).
- Filbin, M. T. Myelin-associated inhibitors of axonal regeneration in the adult mammalian CNS. *Nat. Rev. Neurosci.* **4**, 703–713 (2003).
- Wang, F. & Zhu, Y. The interaction of Nogo-66 receptor with Nogo-p4 inhibits the neuronal differentiation of neural stem cells. *Neuroscience* **151**, 74–81 (2008).
- Maekawa, M. et al. Signaling from Rho to the actin cytoskeleton through protein kinases ROCK and LIM-kinase. *Science* **285**, 895–898 (1999).
- Ridley, A. J. Rho GTPases and actin dynamics in membrane protrusions and vesicle trafficking. *Trends Cell Biol.* **16**, 522–529 (2006).
- Fritz, R. D. et al. A versatile toolkit to produce sensitive FRET biosensors to visualize signaling in time and space. *Sci. Signal.* **6**, rs12 (2013).
- Belyy, A., Merino, F., Sitsel, O. & Raunser, S. Structure of the Lifeact-F-actin complex. *PLoS Biol.* **18**, e3000925 (2020).
- Jung, T. Y. et al. Nogo-A expression in oligodendroglial tumors. *Neuropathology* **31**, 11–19 (2011).
- Orange, J. S. et al. IL-2 induces a WAVE2-dependent pathway for actin reorganization that enables WASp-independent human NK cell function. *J. Clin. Invest.* **121**, 1535–1548 (2011).
- Mace, E. M., Zhang, J., Siminovich, K. A. & Takei, F. Elucidation of the integrin LFA-1-mediated signaling pathway of actin polarization in natural killer cells. *Blood* **116**, 1272–1279 (2010).
- Giger, R. J. et al. Mechanisms of CNS myelin inhibition: evidence for distinct and neuronal cell type specific receptor systems. *Restor. Neurol. Neurosci.* **26**, 97–115 (2008).
- Cao, Z. et al. Receptors for myelin inhibitors: Structures and therapeutic opportunities. *Mol. Cell Neurosci.* **43**, 1–14 (2010).
- Fry, E. J., Ho, C. & David, S. A role for Nogo receptor in macrophage clearance from injured peripheral nerve. *Neuron* **53**, 649–662 (2007).

41. Culley, F. J. et al. Natural killer cell signal integration balances synapse symmetry and migration. *PLoS Biol.* **7**, e1000159 (2009).
  42. Sakai, Y. et al. The Rac activator DOCK2 regulates natural killer cell-mediated cytotoxicity in mice through the lytic synapse formation. *Blood* **122**, 386–393 (2013).
  43. Lang, P. et al. ADP-ribosylation of the ras-related, GTP-binding protein RhoA inhibits lymphocyte-mediated cytotoxicity. *J. Biol. Chem.* **267**, 11677–11680 (1992).
  44. Thauland, T. J., Hu, K. H., Bruce, M. A. & Butte, M. J. Cytoskeletal adaptivity regulates T cell receptor signaling. *Sci. Signal.* **10**, eaah3737 (2017).
  45. Eibert, S. M. et al. Cofilin peptide homologs interfere with immunological synapse formation and T cell activation. *Proc. Natl Acad. Sci. USA* **101**, 1957–1962 (2004).
  46. Stebbins, C. C. et al. Vav1 dephosphorylation by the tyrosine phosphatase SHP-1 as a mechanism for inhibition of cellular cytotoxicity. *Mol. Cell. Biol.* **23**, 6291–6299 (2003).
  47. Peterson, M. E. & Long, E. O. Inhibitory receptor signaling via tyrosine phosphorylation of the adaptor Crk. *Immunity* **29**, 578–588 (2008).
  48. Roycroft, A. & Mayor, R. Molecular basis of contact inhibition of locomotion. *Cell. Mol. Life Sci.* **73**, 1119–1130 (2016).
- Publisher's note** Springer Nature remains neutral with regard to jurisdictional claims in published maps and institutional affiliations.
- Springer Nature or its licensor (e.g. a society or other partner) holds exclusive rights to this article under a publishing agreement with the author(s) or other rightsholder(s); author self-archiving of the accepted manuscript version of this article is solely governed by the terms of such publishing agreement and applicable law.
- © The Author(s), under exclusive licence to Springer Nature America, Inc. 2023

## Methods

### Mice

All mice were randomly bred and/or maintained in a specific-pathogen-free animal facility at 22–26 °C and 40–60% humidity on a 12-h dark–light cycle, with food (Harlan diet, 2018S) and water as needed in the Laboratory Animal Resource Center at KRIBB. C57BL/6N mice (WT) purchased from DooYeol Biotech, NgR1 KO mice (C57BL/6-Rtn4r<sup>tm1cyagen</sup>) purchased from Cyagen Biosciences Inc. and NSIG mice purchased from GHBIO were used for experiments at 6–8 weeks of age. Male mice were randomly used for *in vitro* studies and experiments on antitumor effects *in vivo*. All animal experiments were performed in agreement with the Animal Experimental Ethics Committee of KRIBB.

### Primary NK cell preparation

WT and KO mice were used for *in vitro* experiments with splenocyte harvesting and NK cell isolation. Splenocytes were recovered by grinding the spleens of mice with a 70- $\mu$ m cell strainer (SPL Life Sciences). NK cells were isolated from splenocytes using an mouse NK Cell Isolation Kit (Miltenyi Biotec). Isolated NK cells were cultured in RPMI 1640 (Gibco) containing 10% fetal bovine serum (FBS), 1% penicillin–streptomycin and 10 ng ml<sup>-1</sup> recombinant human IL-2 (hIL-2) (PeproTech). Human UCB was used for NK cell isolation. UCB-NK were isolated using CD3<sup>+</sup> cell depletion with Rosette Sep (StemCell Technologies), density separation with Lymphoprep (StemCell Technologies) and enrichment with a human NK Cell Isolation Kit (Miltenyi Biotec). Human PB was used for NK cell isolation. Blood depleted of platelet-rich plasma was isolated by density gradient centrifugation using Ficoll-Paque (GE Healthcare) to collect PB mononuclear cells, which were collected from the interface layer after centrifugation. PB-NK cells were isolated with a human NK Cell Isolation Kit (Miltenyi Biotec). Cytokine-induced mNK cells were differentiated from CD34<sup>+</sup> hematopoietic stem cells (HSCs). Human CD34<sup>+</sup> HSCs were isolated from UCB using Rosette Sep, Lymphoprep and a human CD34 MicroBead Kit (Miltenyi Biotec). NK cell precursors were differentiated from CD34<sup>+</sup> HSCs in Myelocult H5100 (StemCell Technologies) supplemented with hydrocortisol (10<sup>-6</sup> M), SCF (30 ng ml<sup>-1</sup>), Flt3 (50 ng ml<sup>-1</sup>) ligand and IL-7 (5 ng ml<sup>-1</sup>) for 14 days. mNK cells were differentiated from NK cell precursors by stimulation with hydrocortisol (10<sup>-6</sup> M), IL-21 (30 ng ml<sup>-1</sup>) and IL-15 (30 ng ml<sup>-1</sup>) for 14 days. Mouse and human primary NK cells were maintained under 37 °C and humidified 5% CO<sub>2</sub> conditions.

### Cell lines

YAC-1, CT26, 4T1, B16F10, Jurkat, EL4, AU565 and K562 cells from ATCC were cultured in RPMI 1640 (WelGENE) supplemented with 10% FBS and 1% penicillin–streptomycin (Gibco). NK92 cells from ATCC were cultured in  $\alpha$ -MEM (WelGENE) supplemented with 10% FBS, 1% penicillin–streptomycin and hIL-2 (10 ng ml<sup>-1</sup>). HEK293T cells from ATCC were cultured in Dulbecco's modified Eagle medium (DMEM; WelGENE) supplemented with 10% FBS and 1% penicillin–streptomycin. U87MG cells from ATCC were cultured in minimum essential medium (MEM; WelGENE) supplemented with 10% FBS and 1% penicillin–streptomycin. Cells were incubated under 37 °C and humidified 5% CO<sub>2</sub> conditions.

### Flow cytometry analysis

Cells were washed and stained with antibodies in PBS containing 1% FBS and 2 mM EDTA for 20–30 min in the dark at 4 °C. The following antibodies and dilutions using 5% bovine serum albumin (BSA) in 1 $\times$  PBS with Tween-20 were used for detection of cell surface expression: anti-NgR1-Alexa 647, anti-NK1.1-APC, anti-CD3-Amcyan, anti-CD27-PE, anti-CD11b-PE-Cy7, anti-CD8-PE-Cy7, anti-B220-Pacific Blue, anti-Gr1-Pacific Blue, anti-F4/80-APC, anti-ULBP1-FITC, anti-ULBP2-APC, anti-ULBP3-PE, anti-MIC-A/B-PE, anti-HLA-A/B/C-FITC and anti-p75NTR-FITC. For intracellular IFN- $\gamma$  staining, cells were fixed and permeabilized using a fixation/permeabilization kit (BD

Biosciences) after surface staining and labeled with anti-IFN- $\gamma$ -PE-Cy7 for 20–40 min in the dark at 4 °C. The fluorescent dyes were conjugated to anti-NgR1, anti-LIGO1 and anti-TROY using an Alexa Fluor 647 Antibody Labeling Kit (Invitrogen) for flow cytometry analysis of dye-unconjugated antibodies. Isotype controls containing anti-IgG-APC and anti-IgG-FITC were used as negative controls (Supplementary Table 3). Antibody-labeled cells were analyzed by fluorescence-activated cell sorting (Canto II, BD Biosciences) and data were collected using FlowJo software (Tree Star).

### Cytotoxicity assay

NK cell-mediated cytotoxicity was measured using calcein-AM release assay. Target cells were incubated with calcein-AM (Invitrogen) for 1 h under 37 °C and humidified 5% CO<sub>2</sub> conditions. Calcein-labeled target cells were plated in 96-well round-bottomed plates and then cocultured with serially diluted effector cells at the desired effector:target ratio for the desired incubation time. The calcein released from lysed target cells into the supernatant by effector cells was measured using a multimode microplate reader (Molecular Devices). Maximal and spontaneous release of calcein was simulated by adding 2% Triton X-100 and complete medium to calcein-labeled target cells. The percentage of specific lysis was calculated using the following formula: (experimental release – spontaneous release) / (maximum release – spontaneous release)  $\times$  100%. NEPI-40 or anti-NgR1 was used as a treatment during coculture of effector and target cells to block NgR1.

### Lung metastatic syngeneic mouse model

A lung metastasis model using the B16F10 melanoma cell line was constructed in WT and KO mice. For depletion of NK cells in mice, 100  $\mu$ g of anti-NK1.1 or isotype control in 200  $\mu$ l Dulbecco's PBS (DPBS) was injected intravenously through tails of mice 4 days and 1 day before and 2 days after intravenous injection of B16F10. The CD3<sup>+</sup> NK1.1<sup>+</sup> populations were measured by flow cytometry analysis 5 days before and 4 and 13 days after B16F10 injection. Each mouse was injected intravenously with  $2 \times 10^5$  B16F10 cells on day 0. The body weights of the mice were measured on days 0, 9 and 14 after injection of B16F10. Mice were euthanized 14 days after injection of cancer cells, and their lungs were removed for analysis of metastatic melanoma nodules. The removed lungs were ground with a 70- $\mu$ m cell strainer to analyze the intrapulmonary CD3<sup>+</sup> NK1.1<sup>+</sup> population by flow cytometry.

### Cell-line-derived tumor xenograft mouse model

A xenograft model using the human U87MG glioblastoma cell line was established in NSIG mice lacking T cells, B cells and NK cells. For the development of solid tumors,  $4 \times 10^5$  U87MG cells were implanted subcutaneously into mice on day 0. NK92 cells ( $2.5 \times 10^5$ ) were injected intravenously through the tails of mice 10 and 14 days after U87MG injection, and 300  $\mu$ g of Scram or NEPI-40 in 100  $\mu$ l DPBS were injected intratumorally on days 11 and 15. In the Ctrl group inoculated with only U87MG cells, without NK92 cells, intratumoral injection of 100  $\mu$ l DPBS was performed. From 10 days after plantation of the tumor cells, the width and length of the developed tumor were measured every 4 days with a caliper to calculate the tumor size in mm<sup>3</sup> using the following formula: (width + length)<sup>2</sup> / 2, and body weights were measured at the same time. The tumor size did not exceed 20 mm<sup>2</sup> according to the guidelines of the KRIBB Animal Experimental Ethics Committee. After tumor development, survival of mice was monitored every day during the remainder of the experimental period.

### Immunoblotting

Cells were washed with ice-cold PBS and lysed using cOMplete Lysis-M (Roche), and protein concentrations were measured with a Pierce BCA Protein Assay Kit (Thermo Scientific). Cell lysates containing 10–20  $\mu$ g of proteins were reduced by boiling for 10–15 min using sodium dodecyl sulfate (SDS) sample buffer. Samples were

separated by 8–12% SDS polyacrylamide gel electrophoresis and transferred to a polyvinylidene fluoride membrane (Millipore). Membranes were blocked with 1–5% nonfat milk or BSA in PBS containing 0.05% Tween-20 (Duchefa Biochemie) for 40–60 min at room temperature and then incubated with primary antibodies overnight at 4 °C. Membranes were then washed and incubated with horseradish peroxidase (HRP)-conjugated anti-rabbit or anti-mouse IgG secondary antibody for 40–60 min at room temperature. After washing, the membranes were developed using SuperSignal West Pico PLUS Chemiluminescent Substrate (Thermo Scientific), and immunoblot images were obtained using WSE-6100 LuminoGraph (ATTO). Data were collected using CASanalyzer (ATTO) software. For endogenous RhoA-GTP detection, cells were lysed using cOmplete Lysis-M, and cell lysates were pulled down using a Rho Activation Assay Biochem Kit (Cytoskeleton) according to the manufacturer's protocol. Cell lysates were incubated with Rhotekin, a Rho effector protein that has a Rho-binding domain and is tagged with GST, in a rocker at 4 °C for 1 h. Centrifuged and washed samples were reduced by boiling for 10–15 min using SDS sample buffer, followed by separation and transfer. The following antibodies were used: anti-pLIMK1/2, anti-LIMK2, anti-pCofilin, anti-cofilin, anti-GAPDH, anti-NogoA, anti-NgR1, anti-rabbit IgG-HRP and anti-mouse IgG-HRP (Supplementary Table 3).

### Establishment of stable cell lines

Lifeact-EGFP was transduced into NK92 cells using a lentiviral system for microscopic visual measurement of F-actin in NK cells. For lentivirus generation, HEK293T cells were plated the day before lipoplex-mediated transfection. A mixture of pLenti Lifeact-EGFP (Addgene), VSV-G, pMDLg/pRRE, pRSV-Rev (3:1:1:1 ratio) and TransIT-2020 Transfection Reagent (Mirus) in Opti-MEM I (Gibco) containing 1% penicillin–streptomycin was applied to HEK293T cells dropwise, followed by culture for 3 days in RPMI 1640 supplemented with 10% (FBS) and 1% penicillin–streptomycin. The collected supernatants were centrifuged, filtered through a 0.45 µm filter and resuspended in medium after ultracentrifugation. NK92 cells were infected with titrated virus and protamine sulfate in alpha-MEM supplemented with 10% FBS, 1% penicillin–streptomycin and hIL-2 (10 ng ml<sup>-1</sup>) and incubated for 3 days under 37 °C and humidified 5% CO<sub>2</sub> conditions. Lentivirus-infected and uninfected NK92 cells were selected using blasticidin.

### Transient transfection

K562 cells, NogoA was overexpressed using electroporation. K562 cells (10<sup>6</sup>) and 2.5 µg pCMV NogoA (OriGene) in 100 µl Opti-MEM I containing 1% penicillin–streptomycin were loaded into NEPA electroporation cuvettes (Nepa Gene). After electroporation using NEPA21 Type II (Nepa Gene) according to the manufacturer's protocol, K562 cells were cultured in RPMI 1640 supplemented with 10% FBS and 1% penicillin–streptomycin under 37 °C and humidified 5% CO<sub>2</sub> conditions for 2–3 days. NogoA-overexpressing K562 cells were analyzed for NogoA expression using immunoblotting and flow cytometry and subjected to a cytotoxicity assay. In HEK293T cells, NogoA was overexpressed using lipoplex-mediated transfection. HEK293T cells were plated 1 day before transfection and prepared at a density of about 70% on the day of transfection. A mixture of pCMV NogoA and TransIT-2020 transfection reagent in Opti-MEM I containing 1% penicillin–streptomycin was applied to HEK293T cells dropwise. After 2–3 days, the expression level of overexpressed NogoA in HEK293T cells was analyzed by immunoblotting and flow cytometry, and these cells were used for a cytotoxicity assay. In U87MG cells, NogoA was knocked down using siRNA through lipoplex-mediated transfection. U87MG cells plated 1 day before transfection were treated with a mixture of siRNA for NogoA (siNogoA) and TransIT-X2 Dynamic Delivery System (Mirus) in Opti-MEM I. Transfected U87MG

cells were cultured in DMEM supplemented with 10% FBS and 1% penicillin–streptomycin under 37 °C and humidified 5% CO<sub>2</sub> conditions for 2–3 days. NogoA expression in U87MG cells was analyzed using immunoblotting, and U87MG cells in which NogoA was knocked down were used for cytotoxicity assay. In NK92 cells, NgR1 or cofilin was knocked down by electroporation. NK92 cells (10<sup>6</sup>) and 10 µM siNgR1 or cofilin siRNA (siCofilin) in 100 µl of Opti-MEM I containing 1% penicillin–streptomycin were loaded into NEPA electroporation cuvettes. NK92 cells electroporated with NEPA21 type II were cultured in alpha-MEM supplemented with 10% FBS, 1% penicillin–streptomycin and hIL-2 (10 ng ml<sup>-1</sup>) under 37 °C and humidified 5% CO<sub>2</sub> conditions. After 2–3 days, the expression levels of NgR1 or cofilin after knockdown in NK92 cells was analyzed using immunoblotting or flow cytometry, and these cells were used for cytotoxicity assays. The siRNA sequences were as follows: siNogoA, 5'-GAUUGAAGCGCAAAGCUGA-3'; siNgR1 1, 5'-CGTGACCTCAAACGCCTAGCTGCCAATGA-3'; siNgR1 3, 5'-AGCCTCGACCGTCTCCTACTGCACCAGAA-3'; siCofilin, 5'-GUGUAUAAUGGAAUGUUG-3' (Bioneer).

### Live-cell imaging

A modified Olympus IX 83 epi-fluorescence microscope with a 40X (UPlanFLN, NA = 1.30) objective lens and an ANDOR Zyla 4.2 sCOMS camera was used for imaging experiments. The microscope was automatically controlled by Micro-manager. For live-cell imaging, the microscope stage was equipped with a Chamlide TC incubator system (Live Cell Instrument) maintaining cell culture conditions (37 °C, CO<sub>2</sub> 5%). Acquired images were processed using ImageJ. To observe F-actin dynamics in NK92 cells, NK92 cells expressing Lifeact-GFP were seeded on a glass coverslip, and time-lapse imaging acquiring differential interference contrast and GFP fluorescence was initiated about 15 min after cell seeding. To observe interactions between NK cells and cancer cells, cancer cells were first plated on gelatin-coated coverslips and incubated for 12 h in a tissue culture incubator (37 °C with 5% CO<sub>2</sub>) so that cancer cells could adhere and spread on the substrates. Then, the coverslip containing cancer cells was mounted in a magnetic chamber (Chamlide CF, Live Cell Instrument), and the chamber was loaded on the microscope stage equipped with the incubator system. NK cells were added to the chamber, and time-lapse imaging was initiated 15 min later to allow NK cells to sediment and initiate interactions with the cancer cells. NK cells transfected with Lifeact-GFP and labeled with lysosensor (Thermo Fisher) were used to visualize F-actin and lytic granules, respectively. Killing probability was measured by time-lapse imaging. Total interaction events and killed target cells were directly counted in each field of view.

$$\text{Killing probability} = \frac{\text{number of killing}}{\text{total number of interactions}}$$

### Patient samples

Gene expression and clinical information were downloaded from the GDC data portal (<https://portal.gdc.cancer.gov>). The 9,473 primary tumors from the TCGA data, including 33 cancer types (ACC, BLCA, BRCA, CESC, CHOL, COAD, DLBC, ESCA, GBM, HNSC, KICH, KIRC, KIRP, LAML, LGG, LIHC, LUAD, LUSC, MESO, OV, PAAD, PCPG, PRAD, READ, SARC, SKCM, STAD, TGCT, THCA, THYM, UCEC, UCS and UVM) were used for survival analysis. The log<sub>2</sub>-scaled FPKM values were used for analysis of gene expression.

### CIBERSORT

CIBERSORT was used for mathematical analysis of pan-cancer gene expression data (<https://cibersortx.stanford.edu>)<sup>49</sup>. We used log<sub>2</sub>-scaled FPKM values for deconvolution analysis of available gene expression levels<sup>50</sup>. The gene expression file created based on 9,574 cases was uploaded to CIBERSORT as a mixture file, and CIBERSORT

was run with options for LM22 reference file, 500 permutations and quantile normalization disabled. The quantity of NK cells was calculated as the sum of the quantities of activated NK cells and resting NK cells in the LM22 reference file. The samples for which the quantities of NK cells or CD8 T cells were in the top 10% to 50% with statistical significance ( $P < 0.05$ ) were included in the NK or CD8 T-rich group, and the others were included in the poor group.

### Statistical and survival analysis

One-way or two-way analysis of variance (ANOVA) with Tukey's or Sidak's multiple comparisons test or unpaired two-tailed Student's  $t$  test was used to analyze the significance of findings using GraphPad Prism. The log-rank test and Wald test with 95% confidence intervals were performed to estimate the significance of differences in overall survival. Kaplan–Meier plots and forest plots were used to visualize the results. All survival analyses of clinical information were carried out using R software packages (v.3.6.3). Statistical values are indicated in each figure. Data are represented as mean  $\pm$  s.d. or s.e.m. No statistical methods were used to predetermine sample sizes, but our sample sizes are similar to those reported in previous publications<sup>28,36,42,46</sup>. Data distribution was assumed to be normal, but this was not formally tested. Data collection and analysis were not performed blind to the conditions of the experiments. No data were excluded from the analysis.

### Ethics

This study complies with all applicable codes of ethics. Human studies were approved by the Korea Research Institute of Bioscience and Biotechnology (KRIBB) Institutional Review Board (P01-201610-31-002) and SNU Institutional Review Board (E2102-003-006). For the use of human UCB or PB, informed consent was obtained from the donor through the Cord Blood Bank of Korea or Korea Red Cross Blood Services. Animal studies were approved by the Animal Experimental Ethics Committee (AEC-21016, –21017) and conformed to the Regulations on the management and use of laboratory animals of KRIBB.

### Reporting summary

Further information on research design is available in the Nature Portfolio Reporting Summary linked to this article.

### Data availability

The data supporting the findings of this study are available within the paper and from the corresponding authors upon request. Patient samples, including gene expression and clinical information, were accessed from the GDC data portal (<https://portal.gdc.cancer.gov>). Primary tumor data for survival analysis were from TCGA. Mathematical data for pan-cancer gene expression were analyzed using CIBERSORT (<https://cibersortx.stanford.edu>). Source data are provided with this paper.

## References

49. Newman, A. M. et al. Robust enumeration of cell subsets from tissue expression profiles. *Nat. Methods* **12**, 453–457 (2015).
50. Jin, H., Wan, Y. W. & Liu, Z. Comprehensive evaluation of RNA-seq quantification methods for linearity. *BMC Bioinformatics* **18**, 117 (2017).

## Acknowledgements

We thank Jong Bae Park (National Cancer Center) and Si Rim Lee (KRIBB) for expert technical assistance and experimental trials, respectively. This work was supported by KRIBB Research Initiative Program, the National Research Council of Science & Technology (NST) grant (CAP-18-02-KRIBB to T.-D.K.), the National Research Foundation grant (2022M3E5F1016693 to T.-D.K. and 2020R1A2B5B03001747 to J.D.), and Korea Drug Development Fund (HN21C0117 to T.-D.K.) by the Korea government.

## Author contributions

T.-D.K. and J.D. conceived and designed the study. S.-C.O., S.-E.K. and I.-H.J. acquired, analyzed and interpreted the data. J.D. and S.-E.K. designed the live image data. I.-H.J. and I.-S.C. designed and analyzed bioinformatic data. S.-M.K., S.Y.L., S.L., I.C., S.R.Y. and H.J. provided discussions and advice. S.-C.O., S.-E.K., T.-D.K. and J.D. wrote, reviewed and revised the manuscript. T.-D.K. and J.D. supervised the study and acquired funding.

## Competing interests

The authors declare no competing interests.

## Additional information

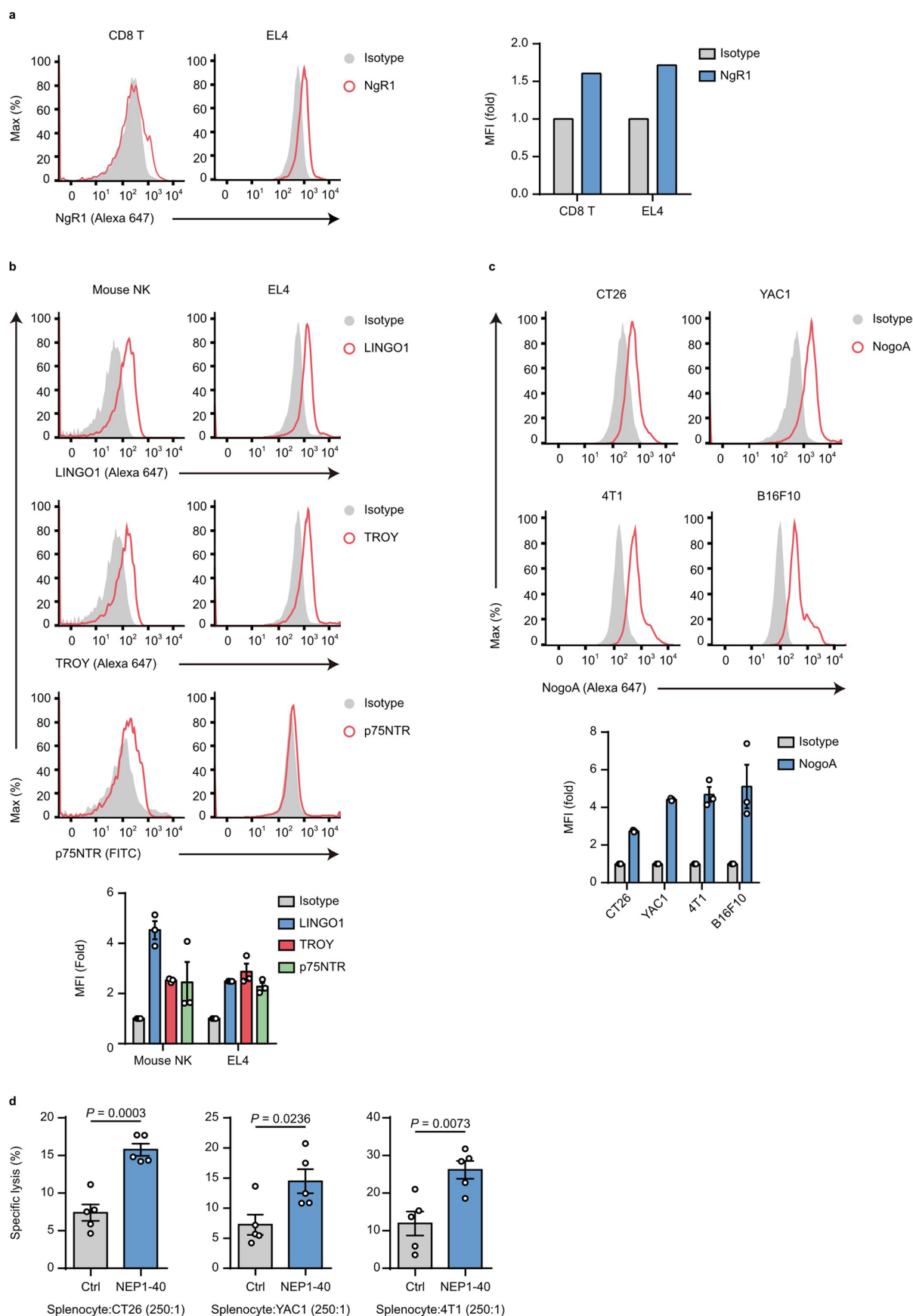
**Extended data** is available for this paper at <https://doi.org/10.1038/s41590-022-01394-w>.

**Supplementary information** The online version contains supplementary material available at <https://doi.org/10.1038/s41590-022-01394-w>.

**Correspondence and requests for materials** should be addressed to Junsang Doh or Tae-Don Kim.

**Peer review information** *Nature Immunology* thanks Daniel Billadeau and the other, anonymous, reviewer(s) for their contribution to the peer review of this work. Primary Handling Editor: N. Bernard in collaboration with the *Nature Immunology* team. Peer reviewer reports are available.

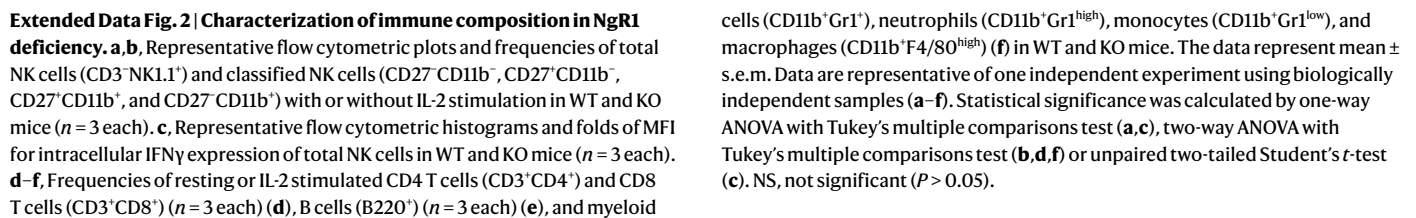
**Reprints and permissions information** is available at [www.nature.com/reprints](http://www.nature.com/reprints).

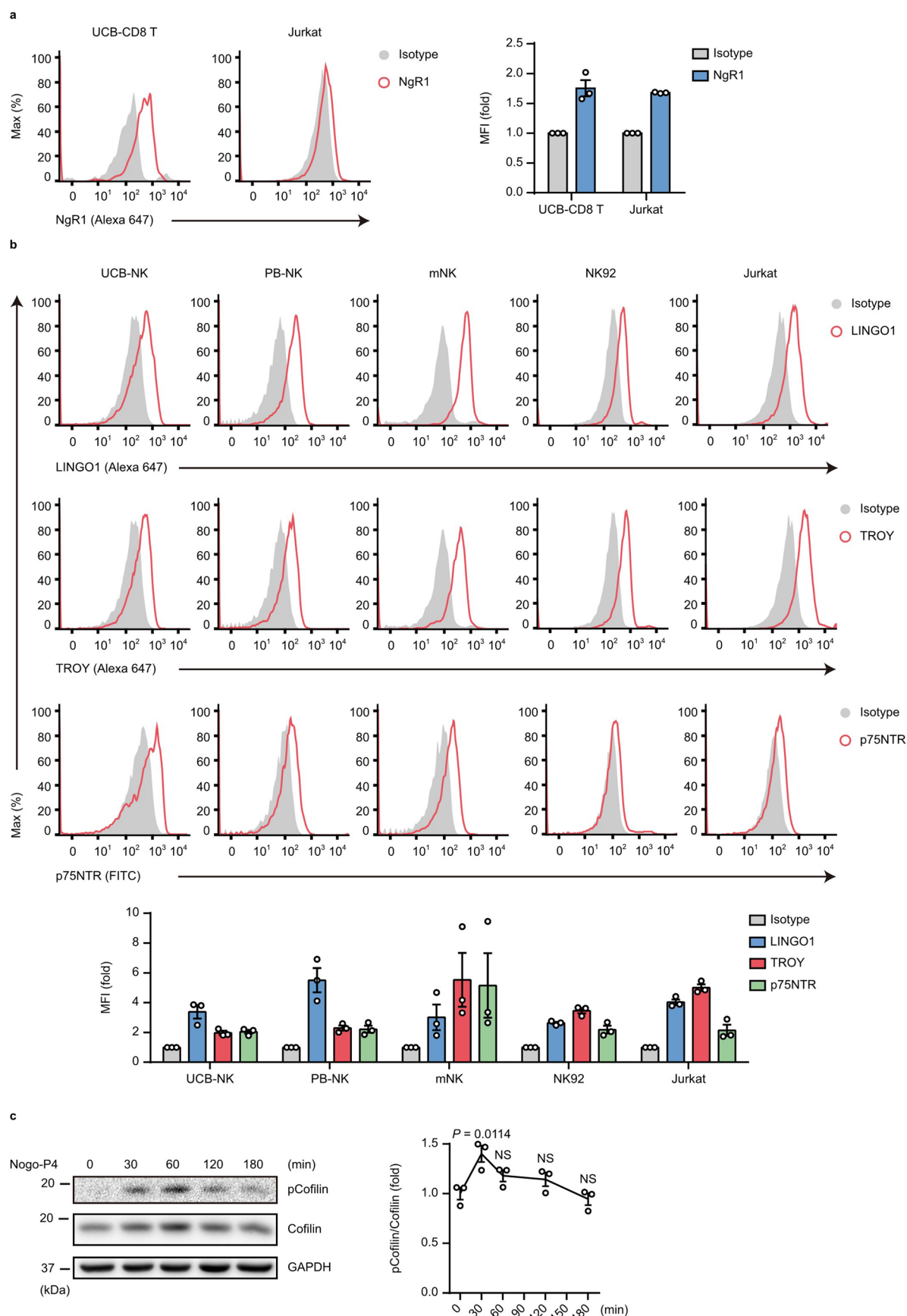


Extended Data Fig. 1 | See next page for caption.

**Extended Data Fig. 1 | Identification of NgR1 in NK cells.** **a**, Representative flow cytometric histograms and folds of MFI for NgR1 expression in splenic CD8 T cells from WT mouse and EL4 cell line ( $n = 1$  each). **b**, Representative flow cytometric histograms and folds of MFI for LINGO1, TROY and p75NTR expression in mouse splenic NK cells and EL4 cell line ( $n = 3$  each). **c**, Representative flow cytometric histograms and folds of MFI for NogoA expression in CT26, YAC-1, 4T1 and

B16F10 cell lines ( $n = 3$  each). **d**, Cytotoxicity analysis on CT26, YAC-1, and 4T1 cells of splenocytes from WT mice with or without NEP1-40 treatment ( $n = 5$  each). In **b–d**, the data represent mean  $\pm$  s.e.m. Data are representative of two independent experiments (**d**). Statistical significance was calculated by unpaired two-tailed Student's *t*-test (**d**).

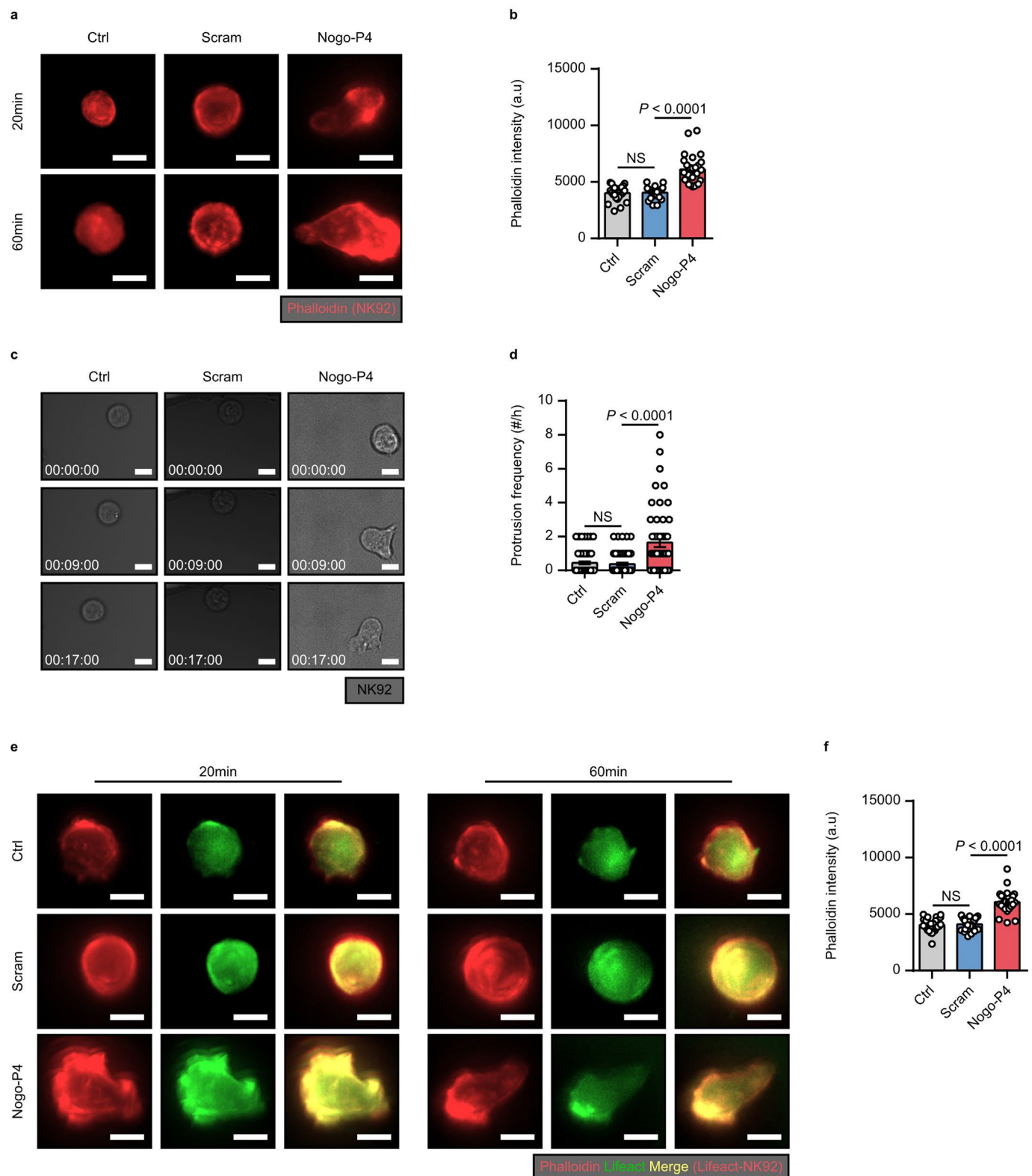




Extended Data Fig. 3 | See next page for caption.

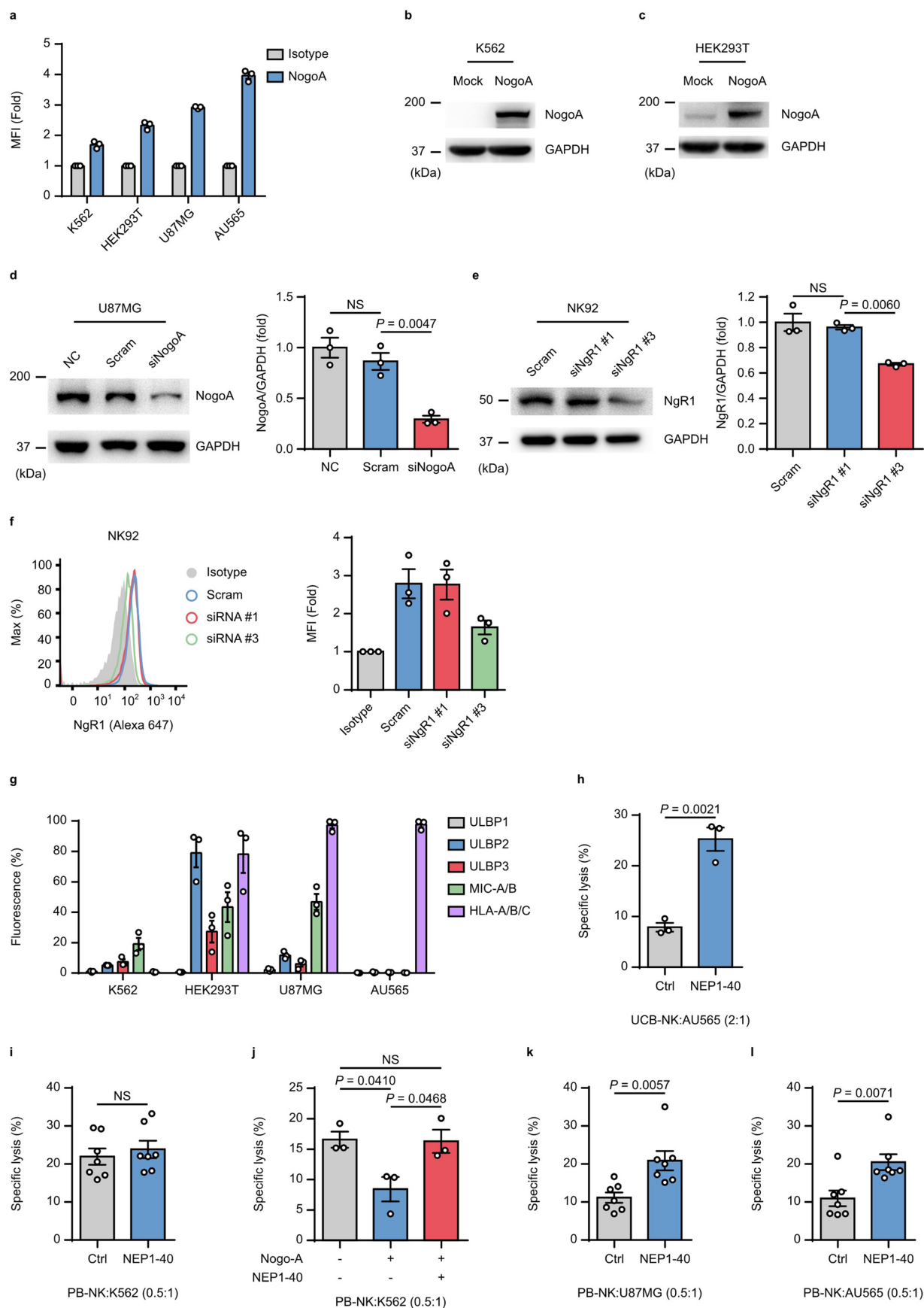
**Extended Data Fig. 3 | NgR1 signals in NK cells. a,b**, Representative flow cytometric histograms and folds of MFI for NgR1 expression in human UCB-CD8 T and Jurkat cell line ( $n = 3$  each) (**a**), and for LINGO1, TROY and p75NTR expression in human UCB-NK, PB-NK, mNK, NK92 and Jurkat cell lines ( $n = 3$  each) (**b**). **c**, Representative immunoblots and quantification analysis of lysate from

human UCB-NK cells treated with Nogo-P4 during indicated time ( $n = 3$  each). The data represent mean  $\pm$  s.e.m. (**a,b**) or mean  $\pm$  s.d. (**c**). Data are representative of two independent experiments (**a,b,c**). Statistical significance was calculated by one-way ANOVA with Tukey's multiple comparisons test (**c**). NS, not significant ( $P > 0.05$ ).



**Extended Data Fig. 4 | Characterization of F-actin dynamics by NgR1. a,** Time-lapse images for fluorescent intensity of phalloidin-stained NK92 cells with untreated (Ctrl), scrambled peptide (Scram) or Nogo-P4 treatment using fluorescence microscopy. Scale bar, 5  $\mu$ m. **b,** Single-cell analysis for phalloidin intensity of NK92 cells ( $n = 26$  each). **c,** Time-lapse images of NK92 cells with untreated (Ctrl), scrambled peptide (Scram) or Nogo-P4 treatment using video microscopy. Scale bar, 5  $\mu$ m. **d,** Single-cell analysis for protrusion frequency of NK92 cells ( $n = 66$  Ctrl;  $n = 63$  Scram;  $n = 53$  Nogo-P4). **e,** Time-lapse images for

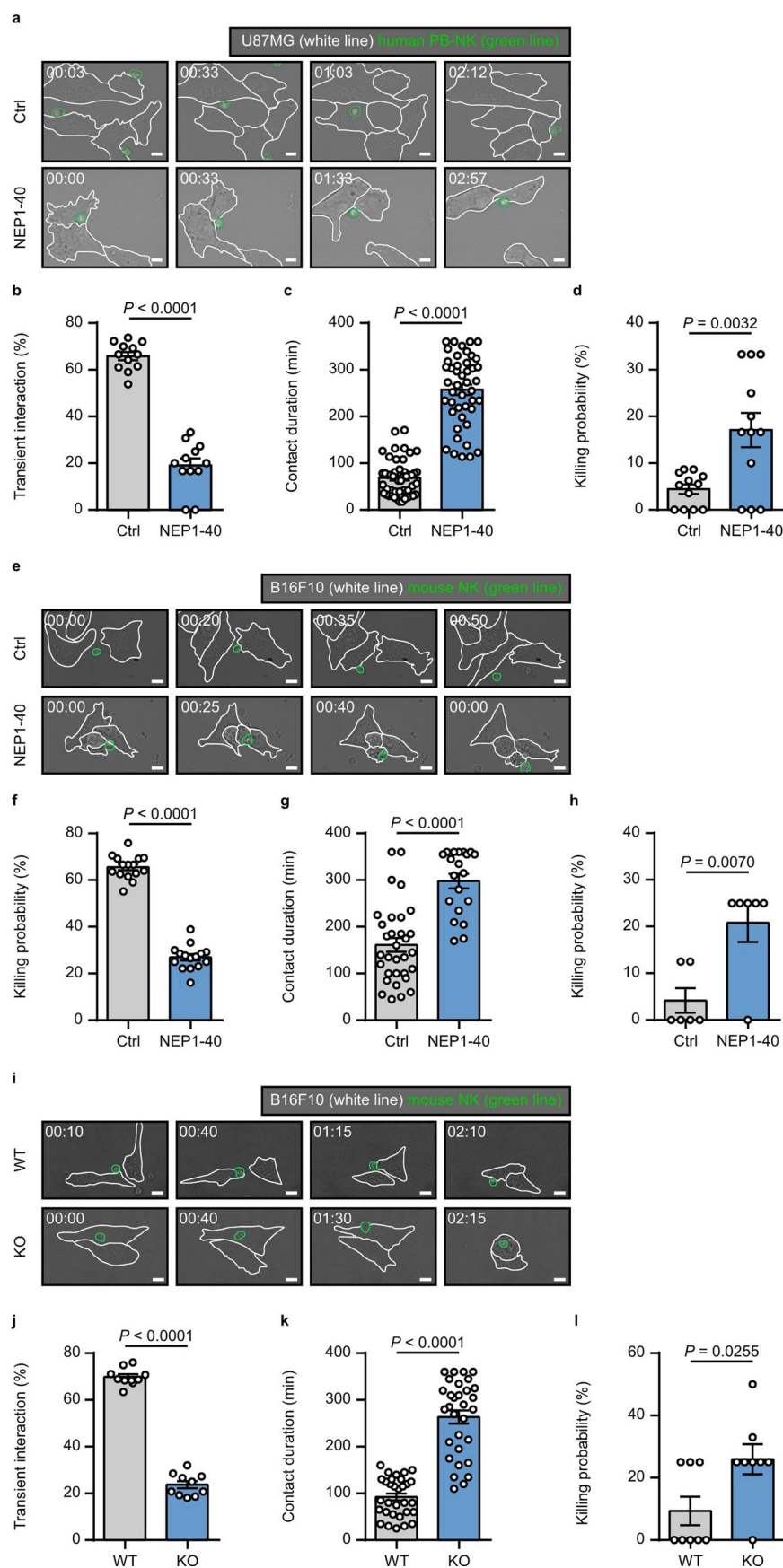
fluorescent intensity of phalloidin-stained NK92 cells expressing Lifeact-GFP with untreated (Ctrl), scrambled peptide (Scram) or Nogo-P4 treatment using fluorescence microscopy. Scale bar, 5  $\mu$ m. **f,** Single-cell analysis for phalloidin intensity of NK92 cells expressing Lifeact-GFP ( $n = 26$  each). The data represent mean  $\pm$  s.e.m. (**b,d,f**). Data are representative of one independent experiment (**b,d,f**). Statistical significance was calculated by one-way ANOVA with Tukey's multiple comparisons test (**b,d,f**). NS, not significant ( $P > 0.05$ ).



Extended Data Fig. 5 | See next page for caption.

**Extended Data Fig. 5 | NgR1 function in NK cell killing.** **a**, Folds of MFI for NogoA expression in K562, HEK293T, U87MG and AU565 cell lines ( $n = 3$  each). **b, c**, Representative immunoblots of lysate from K562 or HEK293T cells overexpressed NogoA. **d**, Representative immunoblots and quantification analysis of lysate from U87MG cells transfected scrambled siRNA (Scram) or NogoA siRNA (siNogoA) ( $n = 3$  each). **e**, Representative immunoblots and quantification analysis of lysate from NK92 cells transfected scrambled siRNA (Scram) or NgR1 siRNA #1 and #3 ( $n = 3$  each). **f**, Representative flow cytometric histograms and folds of MFI for NgR1 expression in NK92 cells transfected scrambled siRNA (Scram), siNgR1 #1 and siNgR1 #3 ( $n = 3$  each). **g**, Folds of MFI for ULBP1, ULBP2, ULBP3, MIC-A/B, and HLA-A/B/C expression in K562, HEK293T,

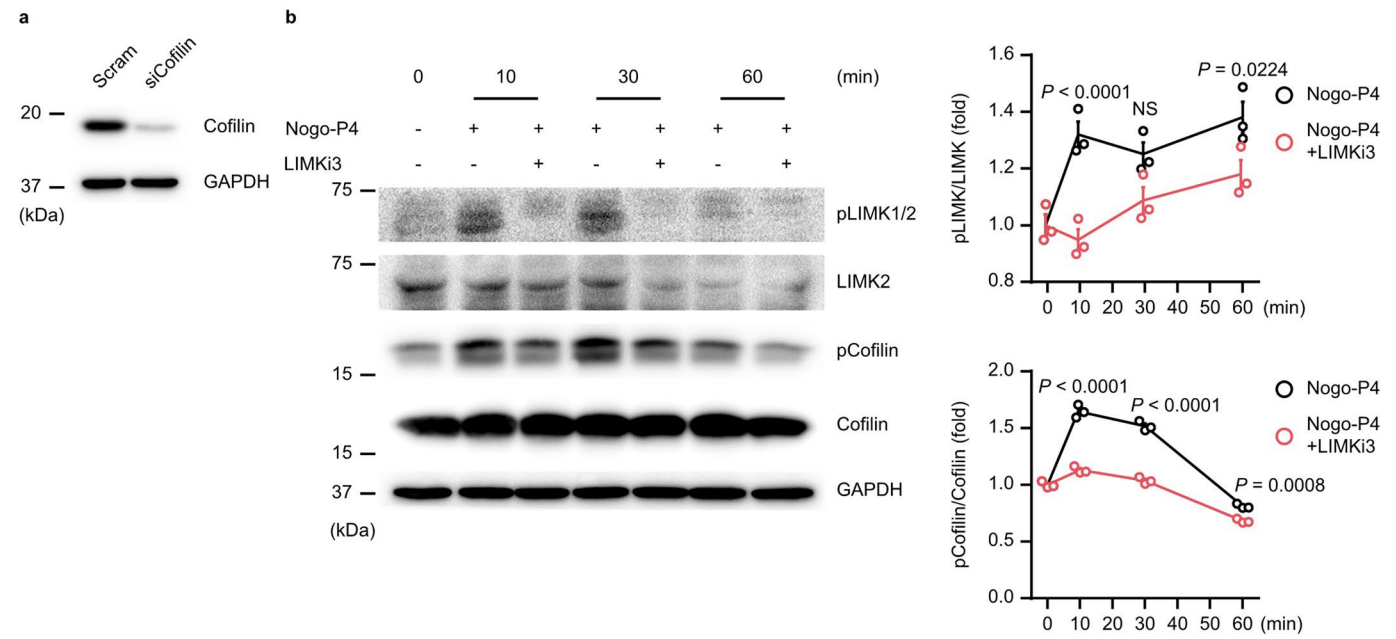
U87MG, and AU565 cell lines ( $n = 3$  each). **h**, Cytotoxicity analysis of human UCB-NK cells to AU565 cells with or without NEPI-40 treatment ( $n = 3$  each). **i-l**, Cytotoxicity analysis of human PB-NK cells to K562 cells ( $n = 7$  each) (**i**), NogoA overexpressed K562 cells ( $n = 3$  each) (**j**), U87MG cells ( $n = 7$ ) (**k**), or AU565 cells ( $n = 7$ ) (**l**) with and without NEPI-40 treatment. The data represent mean  $\pm$  s.e.m. (**a, f-l**) or mean  $\pm$  s.d. (**d, e**). Data are representative of five independent experiments (**k, l**), three independent experiments (**h, i**), two independent experiments (**a, d, e, j**). Statistical significance was calculated by one-way ANOVA with Tukey's multiple comparisons test (**d, e, j**) or unpaired two-tailed Student's *t*-test (**g, i, k, l**). NS, not significant ( $P > 0.05$ ).



Extended Data Fig. 6 | See next page for caption.

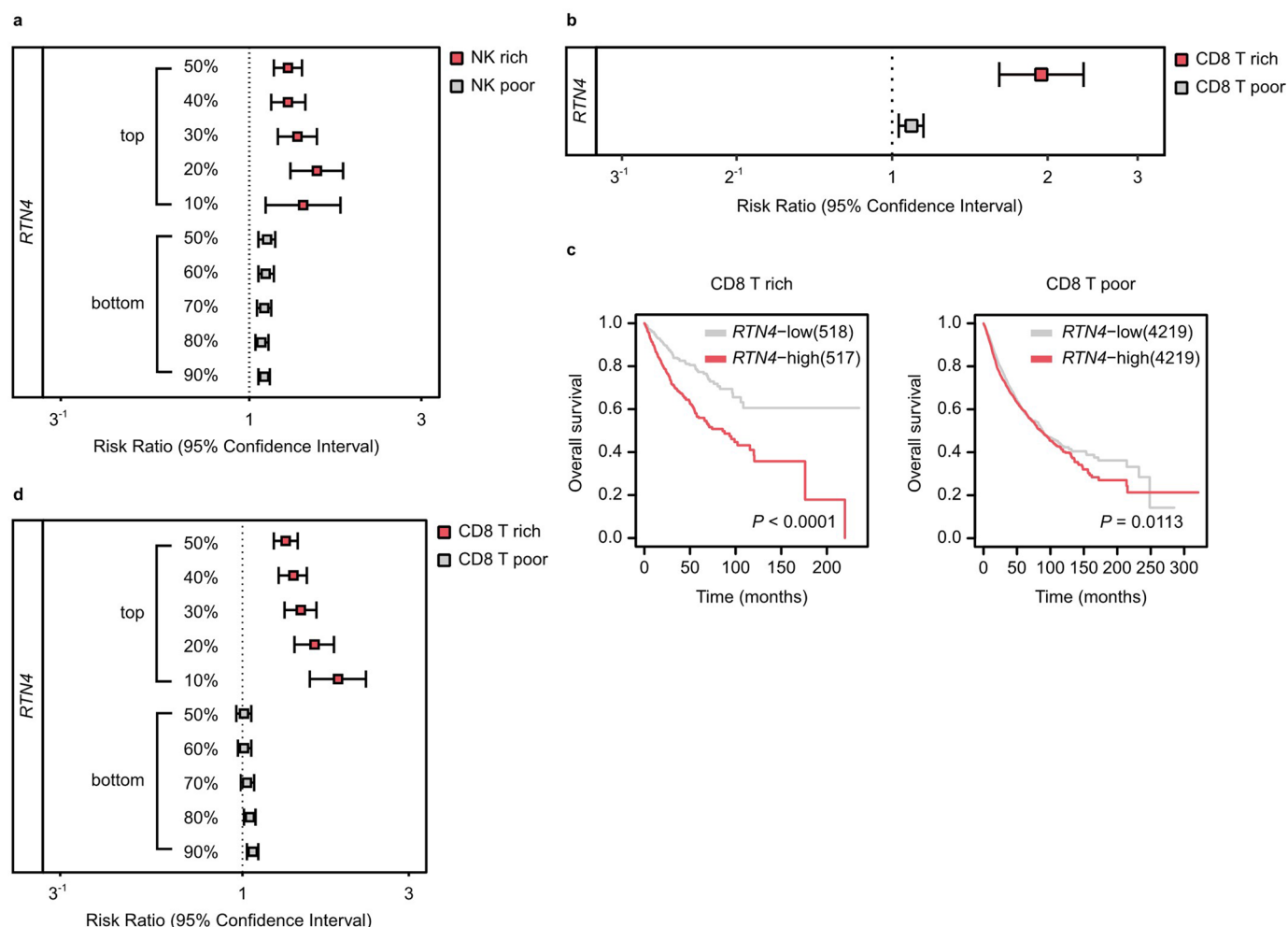
**Extended Data Fig. 6 | Interference of NgR1 in the NK-to-target cell contact.** **a**, Representative time-lapse images of interaction between human PB-NK cells (green border line) and U87MG cells (white border line) with and without NEP1-40. Scale bar, 10  $\mu$ m. **b–d**, Effects of NEP1-40 on NK transient interaction frequencies ( $n = 12$  each) (**b**), contact duration time ( $n = 49$  Ctrl,  $n = 45$  NEP1-40) (**c**) and killing probability ( $n = 12$  each) (**d**). **e**, Representative time-lapse images of interaction between mouse NK cells (green border line) and B16F10 cells (white border line) with and without NEP1-40. Scale bar, 10  $\mu$ m. **f–h**, Effects of NEP1-40 on NK transient interaction frequencies ( $n = 15$  each) (**f**), contact

duration time ( $n = 32$  Ctrl,  $n = 20$  NEP1-40) (**g**) and killing probability ( $n = 6$  each) (**h**). **i**, Representative time-lapse images of interaction between NK cells from WT and KO mice (green border line) and B16F10 cells (white border line). Scale bar, 10  $\mu$ m. **j–l**, Effects of KO on NK transient interaction frequencies ( $n = 10$  each) (**j**), contact duration time ( $n = 31$  each) (**k**) and killing probability ( $n = 8$  each) (**l**). In **b–d, f–h, j–l** the data represent mean  $\pm$  s.e.m. Data are representative of one independent experiments (**b–d, f–h, j–l**). Statistical significance was calculated by unpaired two-tailed Student's *t*-test.



**Extended Data Fig. 7 | Regulation of LIMK–Cofilin signals by NgR1.**  
**a**, Representative immunoblots of lysate from NK92 cells with siCofilin transfection. **b**, Representative immunoblots and quantification analysis of lysate from NK92 cells with and without Nogo-P4 or LIMKi3 treatment

during indicated time ( $n = 3$  each). The data represent mean  $\pm$  s.d. **(b)**, Data are representative of two independent experiments **(b)**. Statistical significance was calculated by two-way ANOVA with Sidak's multiple comparisons test **(b)**. NS, not significant ( $P > 0.05$ ).



**Extended Data Fig. 8 | NgR1 serves as a novel immune checkpoint. a**, Cox hazard ratio of RTN4 expression level stratified by the quantity of infiltrated NK cells at the top 10% to 50% and the bottom 50% to 90% in TCGA pan-cancer. **b**, Cox hazard ratio of RTN4 expression level stratified by the quantity of infiltrated CD8 T cells at the top 20% in TCGA pan-cancer. **c**, Kaplan–Meier plot of RTN4

expression level on top 20% CD8 T-rich and bottom 80% CD8 T-poor groups. **d**, Cox hazard ratio of RTN4 expression level stratified by the quantity of infiltrated CD8 T cells at the top 10% to 50% and the bottom 50% to 90% in TCGA pan-cancer. In **c**, the data represent mean  $\pm$  s.e.m. Statistical significance was calculated by Wald test (**a, b, d**) or log-rank test (**c**).

## Reporting Summary

Nature Portfolio wishes to improve the reproducibility of the work that we publish. This form provides structure for consistency and transparency in reporting. For further information on Nature Portfolio policies, see our [Editorial Policies](#) and the [Editorial Policy Checklist](#).

### Statistics

For all statistical analyses, confirm that the following items are present in the figure legend, table legend, main text, or Methods section.

n/a Confirmed

- ☐ ☒ The exact sample size ( $n$ ) for each experimental group/condition, given as a discrete number and unit of measurement
- ☐ ☒ A statement on whether measurements were taken from distinct samples or whether the same sample was measured repeatedly
- ☐ ☒ The statistical test(s) used AND whether they are one- or two-sided  
*Only common tests should be described solely by name; describe more complex techniques in the Methods section.*
- ☒ ☐ A description of all covariates tested
- ☐ ☒ A description of any assumptions or corrections, such as tests of normality and adjustment for multiple comparisons
- ☐ ☒ A full description of the statistical parameters including central tendency (e.g. means) or other basic estimates (e.g. regression coefficient) AND variation (e.g. standard deviation) or associated estimates of uncertainty (e.g. confidence intervals)
- ☐ ☒ For null hypothesis testing, the test statistic (e.g.  $F$ ,  $t$ ,  $r$ ) with confidence intervals, effect sizes, degrees of freedom and  $P$  value noted  
*Give  $P$  values as exact values whenever suitable.*
- ☒ ☐ For Bayesian analysis, information on the choice of priors and Markov chain Monte Carlo settings
- ☒ ☐ For hierarchical and complex designs, identification of the appropriate level for tests and full reporting of outcomes
- ☒ ☐ Estimates of effect sizes (e.g. Cohen's  $d$ , Pearson's  $r$ ), indicating how they were calculated

*Our web collection on [statistics for biologists](#) contains articles on many of the points above.*

### Software and code

Policy information about [availability of computer code](#)

Data collection	FACS Canto II (BD Biosciences) was used for flow cytometry data collection. Olympus IX83 with a 40X (UPlanFLN, NA=1.30) and ANDOR Zyla 4.2 sComS camera were used for acquisition of microscopy data. WSE-6100 LuminoGraph (ATTO) was used for immunoblotting image collection. FilterMax F3 (Molecular Devices) was used for cytotoxicity assay.
Data analysis	Flow Cytometry data were analyzed by FlowJo V10 (Treestar). CASanalyzer4 (Ver. 2.2.0) (ATTO) was used for immunoblotting data analysis. ImageJ(Ver. fiji) were used for image data analysis. Stastical analysis was conducted using GraphPad Prism V6. R software package (ver. 3.6.3) was used for survival analysis of clinical information.

For manuscripts utilizing custom algorithms or software that are central to the research but not yet described in published literature, software must be made available to editors and reviewers. We strongly encourage code deposition in a community repository (e.g. GitHub). See the Nature Portfolio [guidelines for submitting code & software](#) for further information.

## Data

Policy information about [availability of data](#)

All manuscripts must include a [data availability statement](#). This statement should provide the following information, where applicable:

- Accession codes, unique identifiers, or web links for publicly available datasets
- A description of any restrictions on data availability
- For clinical datasets or third party data, please ensure that the statement adheres to our [policy](#)

Patient samples, including gene expression and clinical information, were from the GDC data portal (<https://portal.gdc.cancer.gov>). Primary tumor data for survival analysis were from The Cancer Genome Atlas (TCGA). A mathematical data of the pan-cancer of gene expression was analyzed using CIBERSORT (<https://cibersortx.stanford.edu>).

## Human research participants

Policy information about [studies involving human research participants and Sex and Gender in Research](#).

Reporting on sex and gender	Because umbilical cord blood was used, only female human specimens were used in the study.
Population characteristics	All donor information was protected by the Institutional Review Board.
Recruitment	Informed consent was obtained from the donor through the Cord Blood Bank of Korea for umbilical cord blood and Korea Red Cross Blood Services for peripheral blood. The blood used for this study was randomized by the Recruitment Entity. Therefore, there are no interventions that could affect the experiment.
Ethics oversight	Human studies were approved by the KIRBB Institutional Review Board (P01-201610-31-002) for umbilical cord blood and SNU Institutional Review Board (E2102-003-006) for peripheral blood.

Note that full information on the approval of the study protocol must also be provided in the manuscript.

## Field-specific reporting

Please select the one below that is the best fit for your research. If you are not sure, read the appropriate sections before making your selection.

☒ Life sciences ☐ Behavioural & social sciences ☐ Ecological, evolutionary & environmental sciences

For a reference copy of the document with all sections, see [nature.com/documents/nr-reporting-summary-flat.pdf](https://nature.com/documents/nr-reporting-summary-flat.pdf)

## Life sciences study design

All studies must disclose on these points even when the disclosure is negative.

Sample size	The sample size was not determined through statistical methods but was chosen by preliminary experiments.
Data exclusions	No data were excluded.
Replication	The replication number of each experiment is stated in each figure.
Randomization	Animals were randomly assigned to each experimental groups to be age-matched.
Blinding	No blinding was used as data were analyzed by each individual responsible for the experiment.

## Behavioural & social sciences study design

All studies must disclose on these points even when the disclosure is negative.

Study description	Briefly describe the study type including whether data are quantitative, qualitative, or mixed-methods (e.g. qualitative cross-sectional, quantitative experimental, mixed-methods case study).
Research sample	State the research sample (e.g. Harvard university undergraduates, villagers in rural India) and provide relevant demographic information (e.g. age, sex) and indicate whether the sample is representative. Provide a rationale for the study sample chosen. For studies involving existing datasets, please describe the dataset and source.

Sampling strategy	<i>Describe the sampling procedure (e.g. random, snowball, stratified, convenience). Describe the statistical methods that were used to predetermine sample size OR if no sample-size calculation was performed, describe how sample sizes were chosen and provide a rationale for why these sample sizes are sufficient. For qualitative data, please indicate whether data saturation was considered, and what criteria were used to decide that no further sampling was needed.</i>
Data collection	<i>Provide details about the data collection procedure, including the instruments or devices used to record the data (e.g. pen and paper, computer, eye tracker, video or audio equipment) whether anyone was present besides the participant(s) and the researcher, and whether the researcher was blind to experimental condition and/or the study hypothesis during data collection.</i>
Timing	<i>Indicate the start and stop dates of data collection. If there is a gap between collection periods, state the dates for each sample cohort.</i>
Data exclusions	<i>If no data were excluded from the analyses, state so OR if data were excluded, provide the exact number of exclusions and the rationale behind them, indicating whether exclusion criteria were pre-established.</i>
Non-participation	<i>State how many participants dropped out/declined participation and the reason(s) given OR provide response rate OR state that no participants dropped out/declined participation.</i>
Randomization	<i>If participants were not allocated into experimental groups, state so OR describe how participants were allocated to groups, and if allocation was not random, describe how covariates were controlled.</i>

## Ecological, evolutionary & environmental sciences study design

All studies must disclose on these points even when the disclosure is negative.

Study description	<i>Briefly describe the study. For quantitative data include treatment factors and interactions, design structure (e.g. factorial, nested, hierarchical), nature and number of experimental units and replicates.</i>
Research sample	<i>Describe the research sample (e.g. a group of tagged <i>Passer domesticus</i>, all <i>Stenocereus thurberi</i> within Organ Pipe Cactus National Monument), and provide a rationale for the sample choice. When relevant, describe the organism taxa, source, sex, age range and any manipulations. State what population the sample is meant to represent when applicable. For studies involving existing datasets, describe the data and its source.</i>
Sampling strategy	<i>Note the sampling procedure. Describe the statistical methods that were used to predetermine sample size OR if no sample-size calculation was performed, describe how sample sizes were chosen and provide a rationale for why these sample sizes are sufficient.</i>
Data collection	<i>Describe the data collection procedure, including who recorded the data and how.</i>
Timing and spatial scale	<i>Indicate the start and stop dates of data collection, noting the frequency and periodicity of sampling and providing a rationale for these choices. If there is a gap between collection periods, state the dates for each sample cohort. Specify the spatial scale from which the data are taken</i>
Data exclusions	<i>If no data were excluded from the analyses, state so OR if data were excluded, describe the exclusions and the rationale behind them, indicating whether exclusion criteria were pre-established.</i>
Reproducibility	<i>Describe the measures taken to verify the reproducibility of experimental findings. For each experiment, note whether any attempts to repeat the experiment failed OR state that all attempts to repeat the experiment were successful.</i>
Randomization	<i>Describe how samples/organisms/participants were allocated into groups. If allocation was not random, describe how covariates were controlled. If this is not relevant to your study, explain why.</i>
Blinding	<i>Describe the extent of blinding used during data acquisition and analysis. If blinding was not possible, describe why OR explain why blinding was not relevant to your study.</i>

Did the study involve field work? ☐ Yes ☐ No

## Field work, collection and transport

Field conditions	<i>Describe the study conditions for field work, providing relevant parameters (e.g. temperature, rainfall).</i>
Location	<i>State the location of the sampling or experiment, providing relevant parameters (e.g. latitude and longitude, elevation, water depth).</i>
Access & import/export	<i>Describe the efforts you have made to access habitats and to collect and import/export your samples in a responsible manner and in compliance with local, national and international laws, noting any permits that were obtained (give the name of the issuing authority, the date of issue, and any identifying information).</i>

Disturbance

Describe any disturbance caused by the study and how it was minimized.

## Reporting for specific materials, systems and methods

We require information from authors about some types of materials, experimental systems and methods used in many studies. Here, indicate whether each material, system or method listed is relevant to your study. If you are not sure if a list item applies to your research, read the appropriate section before selecting a response.

### Materials & experimental systems

n/a	Involved in the study
<input type="checkbox"/>	<input checked="" type="checkbox"/> Antibodies
<input type="checkbox"/>	<input checked="" type="checkbox"/> Eukaryotic cell lines
<input checked="" type="checkbox"/>	<input type="checkbox"/> Palaeontology and archaeology
<input type="checkbox"/>	<input checked="" type="checkbox"/> Animals and other organisms
<input checked="" type="checkbox"/>	<input type="checkbox"/> Clinical data
<input checked="" type="checkbox"/>	<input type="checkbox"/> Dual use research of concern

### Methods

n/a	Involved in the study
<input checked="" type="checkbox"/>	<input type="checkbox"/> ChIP-seq
<input type="checkbox"/>	<input checked="" type="checkbox"/> Flow cytometry
<input checked="" type="checkbox"/>	<input type="checkbox"/> MRI-based neuroimaging

## Antibodies

### Antibodies used

FACS:

anti-B220, V450, clone RA3-6B2, BD Biosciences 560472, Mouse, Flow cytometry

anti-CD11b, PE-Cy7, clone M1/70, invitrogen 25-0112-82, Mouse, Flow Cytometry

anti-CD27, PE, clone LG.3A10, Biolegend 124210, Mouse, Rat, Human, Flow Cytometry

anti-CD3, V500, clone 500A2, BD Biosciences 560771, Mouse, Flow Cytometry

anti-CD8a, PE-Cy7, clone 53-6.7, BD Biosciences 552877, Mouse, Flow Cytometry

anti-F4/80, APC, clone BM8, Biolegend 123115, Mouse, Flow Cytometry

anti-Gr1, V450, clone RB6-8C5, BD Biosciences 560453, Mouse, Flow Cytometry

anti-HLA-A/B/, FITC, clone G46-2.6, BD Biosciences 555552, Human, Flow Cytometry

anti-IFN- $\gamma$ , PE-Cy7, clone XMG1.2, BD Biosciences 557649, Mouse, Flow Cytometry

anti-IgG, Alexa Fluor 488, Cell Signaling Technology 4340, Endogeneous, Rabbit, Flow Cytometry

anti-IgG, Alexa Fluor 647, Cell Signaling Technology 3452, Endogeneous, Rabbit, Flow Cytometry

anti-MIC-A/B, PE, clone DX17, BD Biosciences 560168, Human, Flow Cytometry

anti-NGR1, unconjugated, Alomone labs ANT-008, Human, Mouse, Rabbit, Immunocytochemistry, Immunofluorescence, Indirect flow cytometry, Immunohistochemistry, Live cell imaging, Western blot

anti-NGR1, Alexa 647, clone M5, NOVUS Biologicals NBP2-52675AF647, Human, Mouse, Rabbit, Western blot, ELISA, Flow Cytometry

anti-NK1.1, APC, PK136, BD Biosciences 550627, Mouse, Flow Cytometry

anti-p75NTR, FITC, Alomone labs ANT-007-F, Human, Mouse, Rabbit, Flow Cytometry, Live cell imaging

anti-ULBP1, Alexa fluor 488, clone 170818, R&D Systems FAB1380G, Human, Flow Cytometry

anti-ULBP2, APC, clone 165903, R&D Systems FAB1298A, Human, Flow Cytometry

anti-ULBP3, PE, clone 166510, R&D Systems FAB1517P, Human, Flow Cytometry

in vivo:

anti-NK1.1, unconjugated, clone PK136, BioXCell BE0036, Mouse, in vivo NK cell depletion, Flow Cytometry

Isotype control, unconjugated, clone C1.18.4, BioXCell BE0085, non-reactive isotype-matched control for mouse IgG2a antibodies, in vivo and in vitro applications

Primary antibodies:

anti-Cofilin, clone D3F9, Cell Signaling Technology 5175, Human, Mouse, Rabbit, Monkey, Dog, Western blot, Immunofluorescence

anti-pCofilin (Ser3), clone 77G2, Cell Signaling Technology 3313, Human, Mouse, Rabbit, Monkey, Bovine, Western blot, Immunofluorescence

anti-GAPDH, clone D16H11, Cell Signaling Technology 5174, Human, Mouse, Rabbit, Monkey, Western blot, Immunohistochemistry, Immunofluorescence

anti-LIMK2, clone 8C11, Cell Signaling Technology 3845, Human, Monkey, Western blot

anti-pLIMK1/2 (Thr508/Thr505), Cell Signaling Technology 3841, Human, Western blot

anti-NGR1, Alomone labs ANT-008, Human, Mouse, Rabbit, Immunocytochemistry, Immunofluorescence, Indirect flow cytometry, Immunohistochemistry, Live cell imaging, Western blot

anti-TROY, Alomone labs ANT-033, Human, Mouse, Rabbit, Immunocytochemistry, Immunofluorescence, Live cell imaging, Western blot

anti-LINGO1, Alomone labs ANT-032, Human, Mouse, Rabbit, Immunofluorescence, Immunohistochemistry, Western blot

anti-NogoA, Proteintech 10740-1-AP, Human, Mouse, Rat, Western blot, Immunohistochemistry, Immunofluorescence, Flow cytometry, ELISA

Secondary antibodies:

anti-mouse IgG (H+L), HRP, Jackson Immuno Research 115-035-003, Mouse, Western blot

anti-rabbit IgG (H+L), HRP, Jackson Immuno Research 111-005-003, Rabbit, Western blot

### Validation

The antibodies used are commercially available and validated by the manufacturer (see Antibodies used) and routinely used in the lab.

## Eukaryotic cell lines

Policy information about [cell lines and Sex and Gender in Research](#)

Cell line source(s)	YAC-1, CT26, 4T1, B16F10, Jurkat, EL4, AU565, K562, NK92, HEK293T and U87MG were purchased from ATCC.
Authentication	All cell lines were authenticated basically by ATCC description and experimentally morphological comparison.
Mycoplasma contamination	Cells were tested negative for mycoplasma contamination.
Commonly misidentified lines (See <a href="#">ICLAC</a> register)	No commonly misidentified cells were used.

## Palaeontology and Archaeology

Specimen provenance	<i>Provide provenance information for specimens and describe permits that were obtained for the work (including the name of the issuing authority, the date of issue, and any identifying information). Permits should encompass collection and, where applicable, export.</i>
Specimen deposition	<i>Indicate where the specimens have been deposited to permit free access by other researchers.</i>
Dating methods	<i>If new dates are provided, describe how they were obtained (e.g. collection, storage, sample pretreatment and measurement), where they were obtained (i.e. lab name), the calibration program and the protocol for quality assurance OR state that no new dates are provided.</i>
<input type="checkbox"/> Tick this box to confirm that the raw and calibrated dates are available in the paper or in Supplementary Information.	
Ethics oversight	<i>Identify the organization(s) that approved or provided guidance on the study protocol, OR state that no ethical approval or guidance was required and explain why not.</i>

Note that full information on the approval of the study protocol must also be provided in the manuscript.

## Animals and other research organisms

Policy information about [studies involving animals](#); [ARRIVE guidelines](#) recommended for reporting animal research, and [Sex and Gender in Research](#)

Laboratory animals	C57BL/6N mice (wild type, WT) purchased from DooYeol Biotech, NgR1 KO (KO) mice (C57BL/6-Rtn4rtm1cyagen) purchased from Cyagen Biosciences Inc., NSIG mice purchased from GHBIO were used for experiments at 6–8 weeks of age.
Wild animals	No wild animals were used in the study.
Reporting on sex	Only male mice were used, and gender was not considered in the study.
Field-collected samples	No field-collected samples were used in the study.
Ethics oversight	All mice were bred and/or maintained in the specific-pathogen-free (SPF) animal facility in the Laboratory Animal Resource Center at Korea Research Institute of Bioscience and Biotechnology (KRIBB). Animal studies were approved by the Animal Experimental Ethics Committee (AEC-21016, -21017) and conformed to the Regulations on the management and use of laboratory animals of KRIBB.

Note that full information on the approval of the study protocol must also be provided in the manuscript.

## Clinical data

Policy information about [clinical studies](#)

All manuscripts should comply with the ICMJE [guidelines for publication of clinical research](#) and a completed [CONSORT checklist](#) must be included with all submissions.

Clinical trial registration	<i>Provide the trial registration number from ClinicalTrials.gov or an equivalent agency.</i>
Study protocol	<i>Note where the full trial protocol can be accessed OR if not available, explain why.</i>
Data collection	<i>Describe the settings and locales of data collection, noting the time periods of recruitment and data collection.</i>
Outcomes	<i>Describe how you pre-defined primary and secondary outcome measures and how you assessed these measures.</i>

## Dual use research of concern

Policy information about [dual use research of concern](#)

### Hazards

Could the accidental, deliberate or reckless misuse of agents or technologies generated in the work, or the application of information presented in the manuscript, pose a threat to:

- | No                       | Yes                      |                            |
|--------------------------|--------------------------|----------------------------|
| <input type="checkbox"/> | <input type="checkbox"/> | Public health              |
| <input type="checkbox"/> | <input type="checkbox"/> | National security          |
| <input type="checkbox"/> | <input type="checkbox"/> | Crops and/or livestock     |
| <input type="checkbox"/> | <input type="checkbox"/> | Ecosystems                 |
| <input type="checkbox"/> | <input type="checkbox"/> | Any other significant area |

### Experiments of concern

Does the work involve any of these experiments of concern:

- | No                       | Yes                      |   |
|--------------------------|--------------------------|---|
| <input type="checkbox"/> | <input type="checkbox"/> | Demonstrate how to render a vaccine ineffective                             |
| <input type="checkbox"/> | <input type="checkbox"/> | Confer resistance to therapeutically useful antibiotics or antiviral agents |
| <input type="checkbox"/> | <input type="checkbox"/> | Enhance the virulence of a pathogen or render a nonpathogen virulent        |
| <input type="checkbox"/> | <input type="checkbox"/> | Increase transmissibility of a pathogen                                     |
| <input type="checkbox"/> | <input type="checkbox"/> | Alter the host range of a pathogen  |
| <input type="checkbox"/> | <input type="checkbox"/> | Enable evasion of diagnostic/detection modalities                           |
| <input type="checkbox"/> | <input type="checkbox"/> | Enable the weaponization of a biological agent or toxin                     |
| <input type="checkbox"/> | <input type="checkbox"/> | Any other potentially harmful combination of experiments and agents         |

## ChIP-seq

### Data deposition

- ☐ Confirm that both raw and final processed data have been deposited in a public database such as [GEO](#).
- ☐ Confirm that you have deposited or provided access to graph files (e.g. BED files) for the called peaks.

#### Data access links

May remain private before publication.

For "Initial submission" or "Revised version" documents, provide reviewer access links. For your "Final submission" document, provide a link to the deposited data.

#### Files in database submission

Provide a list of all files available in the database submission.

#### Genome browser session

(e.g. [UCSC](#))

Provide a link to an anonymized genome browser session for "Initial submission" and "Revised version" documents only, to enable peer review. Write "no longer applicable" for "Final submission" documents.

### Methodology

#### Replicates

Describe the experimental replicates, specifying number, type and replicate agreement.

#### Sequencing depth

Describe the sequencing depth for each experiment, providing the total number of reads, uniquely mapped reads, length of reads and whether they were paired- or single-end.

#### Antibodies

Describe the antibodies used for the ChIP-seq experiments; as applicable, provide supplier name, catalog number, clone name, and lot number.

#### Peak calling parameters

Specify the command line program and parameters used for read mapping and peak calling, including the ChIP, control and index files used.

#### Data quality

Describe the methods used to ensure data quality in full detail, including how many peaks are at FDR 5% and above 5-fold enrichment.

#### Software

Describe the software used to collect and analyze the ChIP-seq data. For custom code that has been deposited into a community repository, provide accession details.

## Flow Cytometry

### Plots

Confirm that:

- ☒ The axis labels state the marker and fluorochrome used (e.g. CD4-FITC).
- ☒ The axis scales are clearly visible. Include numbers along axes only for bottom left plot of group (a 'group' is an analysis of identical markers).
- ☒ All plots are contour plots with outliers or pseudocolor plots.
- ☒ A numerical value for number of cells or percentage (with statistics) is provided.

### Methodology

- Sample preparation Detailed sample preparation is described in the Methods section of the manuscript.
- Instrument FACS Canto II (BD Biosciences).
- Software Flow Cytometry data were analyzed by FlowJo V10 (Treestar).
- Cell population abundance At least 10,000 live cells per sample were gated for FACS analysis.
- Gating strategy After gating with FSC-A and FSC-H for singlet, gating was performed with FSC-A and SSC-A to collect live cells. Subsequent gating is described in the Methods section of the manuscript and in the legend of each figure.
- ☐ Tick this box to confirm that a figure exemplifying the gating strategy is provided in the Supplementary Information.

## Magnetic resonance imaging

### Experimental design

- Design type Indicate task or resting state; event-related or block design.
- Design specifications Specify the number of blocks, trials or experimental units per session and/or subject, and specify the length of each trial or block (if trials are blocked) and interval between trials.
- Behavioral performance measures State number and/or type of variables recorded (e.g. correct button press, response time) and what statistics were used to establish that the subjects were performing the task as expected (e.g. mean, range, and/or standard deviation across subjects).

### Acquisition

- Imaging type(s) Specify: functional, structural, diffusion, perfusion.
- Field strength Specify in Tesla
- Sequence & imaging parameters Specify the pulse sequence type (gradient echo, spin echo, etc.), imaging type (EPI, spiral, etc.), field of view, matrix size, slice thickness, orientation and TE/TR/flip angle.
- Area of acquisition State whether a whole brain scan was used OR define the area of acquisition, describing how the region was determined.
- Diffusion MRI ☐ Used ☐ Not used

### Preprocessing

- Preprocessing software Provide detail on software version and revision number and on specific parameters (model/functions, brain extraction, segmentation, smoothing kernel size, etc.).
- Normalization If data were normalized/standardized, describe the approach(es): specify linear or non-linear and define image types used for transformation OR indicate that data were not normalized and explain rationale for lack of normalization.
- Normalization template Describe the template used for normalization/transformation, specifying subject space or group standardized space (e.g. original Talairach, MNI305, ICBM152) OR indicate that the data were not normalized.
- Noise and artifact removal Describe your procedure(s) for artifact and structured noise removal, specifying motion parameters, tissue signals and physiological signals (heart rate, respiration).
- Volume censoring Define your software and/or method and criteria for volume censoring, and state the extent of such censoring.

## Statistical modeling &amp; inference

Model type and settings

Specify type (mass univariate, multivariate, RSA, predictive, etc.) and describe essential details of the model at the first and second levels (e.g. fixed, random or mixed effects; drift or auto-correlation).

Effect(s) tested

Define precise effect in terms of the task or stimulus conditions instead of psychological concepts and indicate whether ANOVA or factorial designs were used.

Specify type of analysis: ☐ Whole brain ☐ ROI-based ☐ BothStatistic type for inference  
(See [Eklund et al. 2016](#))

Specify voxel-wise or cluster-wise and report all relevant parameters for cluster-wise methods.

Correction

Describe the type of correction and how it is obtained for multiple comparisons (e.g. FWE, FDR, permutation or Monte Carlo).

## Models &amp; analysis

n/a | Involved in the study

- ☐ ☐ Functional and/or effective connectivity
- ☐ ☐ Graph analysis
- ☐ ☐ Multivariate modeling or predictive analysis

Functional and/or effective connectivity

Report the measures of dependence used and the model details (e.g. Pearson correlation, partial correlation, mutual information).

Graph analysis

Report the dependent variable and connectivity measure, specifying weighted graph or binarized graph, subject- or group-level, and the global and/or node summaries used (e.g. clustering coefficient, efficiency, etc.).

Multivariate modeling and predictive analysis

Specify independent variables, features extraction and dimension reduction, model, training and evaluation metrics.